Check for updates

Reinforced Concrete Core Wall Buildings with Modified Friction-Based Force-Limiting Connections: Connection Design Considerations and 3D Response to Bidirectional Ground Motions

Kyoungyeon Lee, S.M.ASCE[1]; Georgios Tsampras, Ph.D., M.ASCE[2]; and C. Franco Mayorga, S.M.ASCE[3]

Abstract: This paper discusses the seismic response of a three-dimensional (3D) 18-story reinforced concrete core wall building model with modified friction-based force-limiting connections (Modified FDs) between the floors and reinforced concrete core wall. One set of design parameters that define the predetermined discrete variable friction force-displacement response of the Modified FDs was determined using Pareto front analysis. The Pareto front analysis utilized results from systematic parametric numerical earthquake simulations of two-dimensional (2D) building models and results from a practical force-based design method for force-limiting connections. A 3D model of an 18-story reinforced concrete core wall building was developed with experimentally calibrated wall piers and the Modified FDs considering the determined set of design parameters. Thirteen design-level far-field bidirectional ground motions were considered as seismic excitations. The use of the Modified FDs demonstrates a reduction in the peak torsional moment and base strain responses in the wall piers. A statistical analysis indicates a reasonable range of relative displacement between the floors and the wall piers. The use of the Modified FDs does not increase the expected postearthquake residual drift responses in the building system. The peak floor acceleration and base shear responses are limited, attributed to the controlled inelastic shear-dominant higher-mode responses enabled by the Modified FDs. **DOI: 10.1061/JSENDH.STENG-13609.** *© 2024 American Society of Civil Engineers.*

Author keywords: Modified friction-based force-limiting connection; Reinforced concrete core wall system; Multistory buildings; Higher-mode responses; Three-dimensional (3D) seismic response; Design of force-limiting connections.

Introduction

Higher-Mode Dynamic Response of Reinforced Concrete Multistory Buildings with Core Wall System

A reinforced concrete core wall system is a popular seismic force-resisting system (SFRS) for multistory buildings (Ali and Moon 2007; Christopoulos and Zhong 2022; Moehle 2006). The core wall system typically consists of coupled walls oriented in two orthogonal directions in the floor plan. Coupled walls are structural walls connected by coupling beams along the height of the structure. Compared with uncoupled cantilever walls, the coupled wall system is more beneficial because of its additional energy dissipation capacity in the coupling beams designed to deform plastically (ACI 2019; Paulay and Priestley 1992) and its larger lateral stiffness due to the coupling action between the wall piers and the coupling beams (Moehle et al. 2011; Priestley et al. 2007). Thus, the energy dissipation capacity and lateral stiffness of the core wall system, along with its lateral stability compared to planar walls, make the core wall a desirable system for multistory buildings.

As buildings get taller and/or slenderer, the contribution of the second- and higher-mode dynamic responses to the total dynamic response of the building increases. This phenomenon is often referred to as the higher-mode effects. Multistory buildings with core wall SFRS are assumed to have inelastic deformations located at the base of the core wall and at the coupling beams, while the rest of the structure remains elastic. The inelastic response at the wall base modifies the state of stiffness of the building and reduces the acceleration and the force responses related to the flexure-dominant first-mode response. However, the inelastic response at the wall base does not limit the shear-dominant second- or higher-mode responses (Christopoulos and Zhong 2022; Pennucci et al. 2015; Calugaru and Panagiotou 2012; Panneton et al. 2006). The second- or higher-mode responses continue to increase as the earthquake intensity increases, as long as the rest of the structural components remain linear elastic (Pennucci et al. 2015; Calugaru and Panagiotou 2012). Therefore, applying the same reduction factor to the responses related to the first mode and higher modes of a structure in the reduced response spectrum analysis can underestimate the higher-mode effects for structures with significant higher-mode participation (Zhong and Christopoulos 2022a; Pennucci et al. 2015). The underestimation of demands related to higher-mode responses can lead to seismic amplification of story shear forces and floor accelerations, resulting in undesirable damage, such as shear-induced cracking or damage in the acceleration-sensitive nonstructural

[1]Ph.D. Student, Dept. of Structural Engineering, Univ. of California San Diego, 9500 Gilman Dr., La Jolla, CA 92093 (corresponding author). ORCID: https://orcid.org/0000-0002-6184-8027. Email: kyl008@ucsd.edu

[2]Assistant Professor, Dept. of Structural Engineering, Univ. of California San Diego, 9500 Gilman Dr., La Jolla, CA 92093. ORCID: https://orcid.org/0000-0001-8255-3415. Email: gtsampras@ucsd.edu

[3]Ph.D. Student, Dept. of Structural Engineering, Univ. of California San Diego, 9500 Gilman Dr., La Jolla, CA 92093. ORCID: https://orcid.org/0009-0009-2471-5207. Email: cfmayorg@ucsd.edu

Note. This manuscript was submitted on December 28, 2023; approved on April 15, 2024; published online on November 22, 2024. Discussion period open until April 22, 2025; separate discussions must be submitted for individual papers. This paper is part of the ***Journal of Structural Engineering***, © ASCE, ISSN 0733-9445.

Downloaded from ascelibrary.org by University of California, San Diego on 12/17/24. Copyright ASCE. For personal use only; all rights reserved.

components. The actual seismic demands in these systems often exceed the expected designed values calculated based on the intended ductility of the coupled wall structures, even after the formation of the base inelastic flexural mechanism (Christopoulos and Zhong 2022; Calugaru and Panagiotou 2012; Fatemi et al. 2020; Panneton et al. 2006).

Past Research toward Mitigating Higher-Mode Effects on Core Wall System

Researchers have studied systems that can reduce the higher-mode effects in multistory buildings: multiple plastic hinges (Panagiotou and Restrepo 2009) or multiple rocking mechanisms (Wiebe and Christopoulos 2009; Wiebe et al. 2013a, b) along the height of structural walls; steel coupling beams combined with various types of dampers, including friction, metallic, and viscoelastic dampers (Cui et al. 2022a; Chung et al. 2009; Christopoulos and Montgomery 2013; Li et al. 2019; Qu et al. 2020; Cui et al. 2022b); core wall buildings with base isolation system (Calugaru and Panagiotou 2014; Komuro et al. 2005); and core wall buildings with flexural (i.e., rocking) and shear (i.e., base isolation) inelastic mechanisms at their base (Calugaru 2013; Zhong and Christopoulos 2022b, 2023a, b; Kent et al. 2023; Tong and Christopoulos 2020, 2021).

Another way to limit the shear-dominant higher-mode response is by introducing inelastic force-displacement responses in the connections between the gravity load-resisting system (GLRS) and the SFRS. Skinner et al. (1974) inspired the concept of separating the GLRS from the SFRS and connecting the two systems with hysteretic dampers. This concept allows for controlled relative movement between the GLRS and the SFRS while distributing the inelastic deformation in the dampers placed directly in the path of the seismic-induced horizontal inertial forces over the height of a building. This concept was further studied by Key (1984), Luco and De Barros (1998), Mar and Tipping (2000), Johnston et al. (2014), and Crane (2004), and their numerical analyses and experimental tests showed a reduction in the force and acceleration responses at all floor levels. A detailed literature review on this concept is presented by Tsampras et al. (2016b).

This concept of limiting the seismic-induced responses through deformable connections between the GLRS and SFRS continued. Fleischman et al. (2015) introduced the system with force-limiting connections between the GLRS and the SFRS composed of planar vertical structural elements (planar SFRS). The force-limiting connections allow the movement of the GLRS relative to the SFRS and transfer controlled forces between the two systems. Tsampras et al. (2016b) presented the development of the force-limiting connections for buildings with planar SFRS. The force-limiting connections consist of two components: a friction device or a buckling-restrained brace and low-damping rubber bearings. The friction device or the buckling-restrained brace has limited-strength hysteretic properties. The low-damping rubber bearings stabilize the out-of-plane motion of the planar SFRS and provide postelastic stiffness to prevent excessive connection deformation. The numerical earthquake simulations of a 12-story reinforced concrete planar wall building model with force-limiting connections showed that the nonlinearity provided by the force-limiting connections along the height of the structure mitigates the higher-mode effects, reducing the magnitude and variability of the seismic-induced force and acceleration responses of the building, compared with conventional buildings with planar SFRS. Tsampras and Sause (2014a, b) and Tsampras et al. (2016a, 2017) conducted experimental validation of full-scale force-limiting connections. Fleischman et al. (2014) and Zhang et al. (2018) performed a shake table test of a half-scale 4-story reinforced concrete planar wall building with force-limiting connections. Tsampras and Sause (2022) proposed a force-based design method to determine the limiting force of the force-limiting connections along the height of the structure, accounting for the second- and higher-mode seismic responses. Force-limiting connections designed using this method were numerically simulated in 12-, 8-, and 4-story reinforced concrete planar wall building models, and resulted in acceptable seismic responses and reasonable connection deformation demands. Mayorga and Tsampras (2024) demonstrated that the use of the force-limiting connections designed with this force-based design method reduces the effect of the uncertainty in the longitudinal reinforcing steel model parameters on the floor total acceleration and force response in reinforced concrete planar wall buildings.

Force-Limiting Connections on Core Wall System

Considering that the core wall system is one of the most popular SFRS for multistory buildings, it is beneficial to extend the concept of the force-limiting connections developed for buildings with planar SFRS [Fig. 1(a)] to the connections between the GLRS and core wall SFRS. However, the three-dimensional (3D) seismic-induced kinematic requirements in the connections between the GLRS and core wall SFRS are different from the kinematic requirements in the connections between the GLRS and planar SFRS.

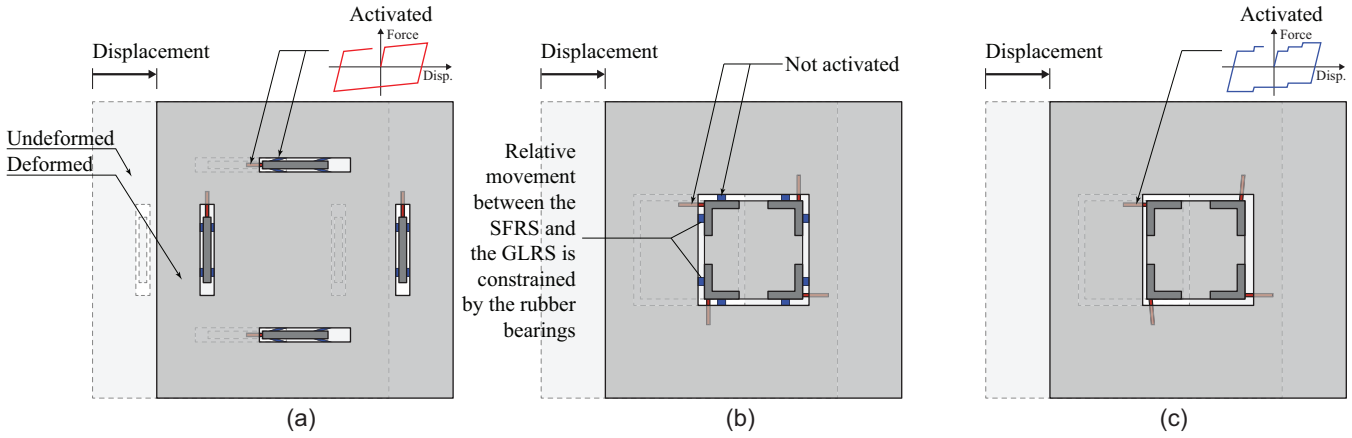


Fig. 1. (Color) (a) Planar wall building with force-limiting connections; (b) core wall building with force-limiting connections developed for planar wall buildings (to demonstrate the limitations); and (c) core wall building with the Modified FDs.

Downloaded from ascelibrary.org by University of California, San Diego on 12/17/24. Copyright ASCE. For personal use only; all rights reserved.

Thus, the force-limiting connections developed for buildings with planar SFRS have been modified to accommodate the difference in the kinematic requirements and allow their use in buildings with core wall SFRS.

Fig. 1(b) shows the force-limiting connections developed for buildings with planar SFRS, without modification, placed on a building with core wall SFRS to explain the limitations induced by the kinematic requirements. The building with core wall SFRS is deforming due to the seismic-induced effects, but the rubber bearings with high compressive stiffness constrain the relative movement between the GLRS and core wall SFRS. The force between the GLRS and core wall SFRS is expected to be transferred primarily through the rubber bearings in an uncontrolled manner, which prevents the initiation of the sliding of the friction devices. Therefore, force-limiting connections without rubber bearings have to be used in buildings with core wall SFRS to allow the relative movement between the GLRS and core wall SFRS, and to activate the friction devices. As mentioned in the previous section, the rubber bearings in the force-limiting connection for buildings with planar SFRS serve two purposes: to stabilize the out-of-plane motion of the planar SFRS and to provide postelastic stiffness to the force-limiting connections. The core wall is a laterally stable system, which eliminates the need for stabilizing from the rubber bearings. However, the postelastic stiffness of the force-limiting connections is essential to prevent excessive connection deformation. Thus, the friction device is modified to have a novel force-displacement response with predetermined discrete variable friction forces that results in an effective equivalent postelastic stiffness. Modified Friction Device (Modified FD) is the term used to distinguish the modified friction device developed for buildings with core wall SFRS from the friction device with constant friction force developed for buildings with planar SFRS. Fig. 1(c) shows the Modified FDs placed on a building with core wall SFRS. The novel force-displacement response of the Modified FD allows the relative movement between the GLRS and core wall SFRS, and enables the limitation of forces without excessive deformation demands.

The development of the physical embodiment of the Modified FD is presented by Chen et al. (2023). Figs. 2(a and b) show the assembled and exploded view of the prototype of the Modified FD, respectively. Fig. 2(c) shows the expected force-displacement response of the Modified FD defined by the design parameters F_1, F_2, F_3, D_1, D_2, K_1, K_2, and K_3. Note that F_1, $F_1 + F_2$, and $F_1 + F_2 + F_3$ represent the predetermined friction forces, with the corresponding elastic stiffnesses K_1, K_2, and K_3, respectively. Also, D_1 and D_2 represent the predetermined displacement at which $F_1 + F_2$ and $F_1 + F_2 + F_3$ are developed, respectively. Chen et al. (2022, 2023) and Lee et al. (2022) conducted a preliminary 3D numerical earthquake simulation of an 18-story core wall building model with the Modified FDs, designed based on one set of prototype design parameters, subjected to one design-level ground motion. To improve the assessment of the seismic response of a core wall building model using the Modified FDs, extensive parametric numerical earthquake simulations are required. More specifically, the effect of the Modified FD design parameters on the seismic response of a core wall building model needs to be studied to define the design space of the design parameters of the Modified FDs. Also, the effect of the characteristics of bidirectional strong ground motions in the 3D seismic response of a core wall building model with the Modified FDs needs to be studied.

Scope of Study

The objective of this paper is (1) to explore the design space and determine one set of the design parameters of the Modified FD, and (2) to assess the seismic response of a 3D 18-story core wall building model with the Modified FDs. One set of the design parameters of the Modified FD that result in an improved seismic response of a building model was determined using Pareto front analysis. The Pareto front analysis utilized results from systematic parametric numerical earthquake simulations of two-dimensional (2D) building models and results from a practical force-based design method for force-limiting connections. A 3D model of an 18-story reinforced concrete core wall building was developed with experimentally calibrated wall piers and the Modified FDs considering the determined set of design parameters. Numerical earthquake simulations of the 3D 18-story reinforced concrete core wall building were performed considering 13 design-level far-field bidirectional ground motions. The seismic response of the building model with the Modified FDs was compared with the seismic response of the building model with conventional monolithic connections. The seismic response of the building model with the Modified FDs was also compared with the seismic response of the building model with force-limiting connections developed for buildings with planar SFRS and the seismic response of the building model with force-limiting connections with only friction devices and no rubber bearings. The comparative analysis was performed focusing on the floor total acceleration, SFRS story shear, SFRS story torsional moment, story drift ratio, story torsional drift ratio, residual drift ratio responses, and the maximum and minimum strain responses at the wall base. A detailed assessment of the higher-mode effects in the total dynamic response of the building was performed.

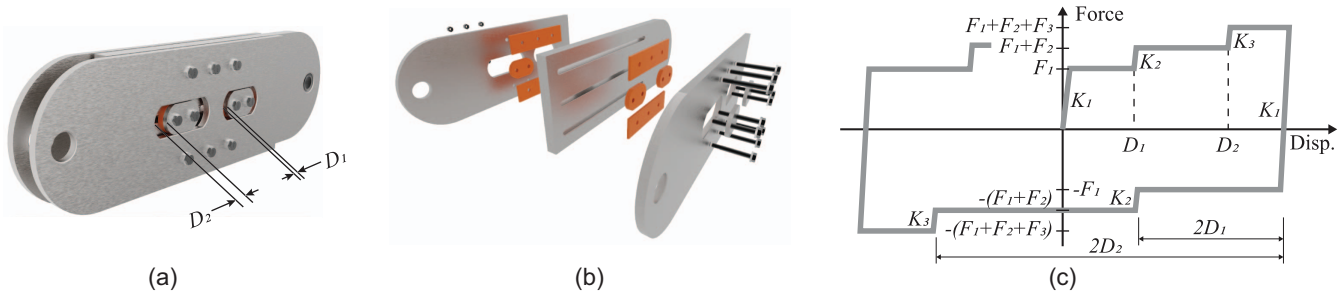


Fig. 2. (Color) (a) Assembled view; (b) exploded view of the prototype of the Modified FD; and (c) expected force-displacement response of the Modified FD.

Downloaded from ascelibrary.org by University of California, San Diego on 12/17/24. Copyright ASCE. For personal use only; all rights reserved.

Numerical Model of the 18-Story Core Wall Building

Geometry and Design of the 18-Story Core Wall Building

A 3D 18-story core wall building designed by Tauberg et al. (2019) was adopted in this study to perform earthquake numerical simulations. Figs. 3(a–c) show the typical floor plan, section, and schematic illustration of the building. The typical story height is 3,048 mm. Twelve gravity columns are located along the edge of the slab. The core wall, which consists of four L-shaped wall piers connected by coupling beams, is located at the center of the floor plan. The wall length is 2,743 mm. The wall thickness varies along the height of the building: 610 mm at story levels from 1 to 5; 508 mm at story levels from 6 to 8; and 406 mm at story levels from 9 to 18. The aspect ratio of the coupling beams is 3.0, with a length of 2,286 mm and a height of 762 mm. The slab thickness is 203 mm. The building is designed according to ASCE 7-16 (ASCE 2016) and ACI 318-14 (ACI 2014), including the wall shear amplification due to higher-mode effects and drift capacity per ACI 318-19 (ACI 2019). The building is designed using the design coefficients and factors of the reinforced concrete ductile coupled walls per ASCE 7-22 (ASCE 2022) and using the design spectral acceleration at short periods $(S_{DS}) = 1.0g$ and at a period of 1 s $(S_{D1}) = 0.6g$.

Numerical Model of the 18-Story Core Wall Building

A numerical model of the 18-story core wall building was developed in OpenSees (McKenna et al. 2010). Fig. 4(a) shows the schematic illustration of the 18-story core wall building with separated GLRS and SFRS, connected with either conventional monolithic connections or force-limiting connections represented by the red lines in the schematic illustration. Figs. 4(b and c) show a schematic overview of the numerical model and its elements in the typical story, respectively. One wall pier element represents one L-shaped wall pier on one story and is located at the geometric center of each wall section. One gravity column element represents three gravity columns and was modeled using the elastic beam-column element with cracked section properties according to ACI 318-19 (ACI 2019). Rigid links connect the geometric centroids of the elements, enforcing the two nodes at their ends to move as a rigid body. The flexibility of the foundation of the building was not modeled. The wall pier elements and the gravity column elements were assumed to have fixed and pinned boundary conditions at their base, respectively. Geometric nonlinearities were simulated to account for the effect of large displacements (relative to the length of the elements) in the response of the building model. The inelastic responses of the wall piers, the coupling beams, and the force-limiting connections were simulated. The responses of the remaining structural elements in the building model were assumed to be linear elastic. The modeling approach of the coupling beams was adopted from Tauberg et al. (2019). The modeling approach of the wall piers and the force-limiting connections are presented in the following sections.

The slab enclosed by the wall piers is termed the SFRS diaphragm. The slab outside the wall piers is termed the GLRS diaphragm. The SFRS diaphragm connects the four wall pier elements, and the GLRS diaphragm connects the four gravity column elements. The SFRS diaphragm is connected to the GLRS diaphragm with corotational truss elements that simulate either conventional monolithic connections or force-limiting connections. Both the GLRS and SFRS diaphragms have orders of magnitude larger in-plane flexural stiffness and orders of magnitude smaller out-of-plane flexural stiffness relative to the flexural stiffness of other elements. The GLRS diaphragm does not allow in-plane axial deformation between the gravity column elements as a rigid diaphragm. The SFRS diaphragm allows in-plane axial deformation between the wall pier elements to represent the voids in the core and to ensure the axial load transfer through the coupling beams. The seismic mass was calculated according to FEMA P695 (FEMA 2009). The seismic mass inside and outside the core on each floor level were equally divided and applied at the top node of the four wall pier elements and the four gravity column elements, respectively.

Core Wall Pier Numerical Model

The core wall piers were modeled using force-based nonlinear elements with fiber sections. Fig. 5(a) shows a typical wall pier element with five integration points. The four wall piers on each story have the same reinforcement detailing. The wall pier fiber sections consist of fibers that simulate the stress-strain response of concrete and steel materials. Fig. 5(b) shows the fiber section on floor Level 12. Due to the aspect ratio of the wall piers, the shear deformation of the wall piers was assumed to be small compared to the flexural deformation under design-level earthquake ground motions and therefore was ignored. Bond slip and bar buckling of the longitudinal reinforcement of the wall piers were not expected to dominate the seismic response of wall piers in the building model

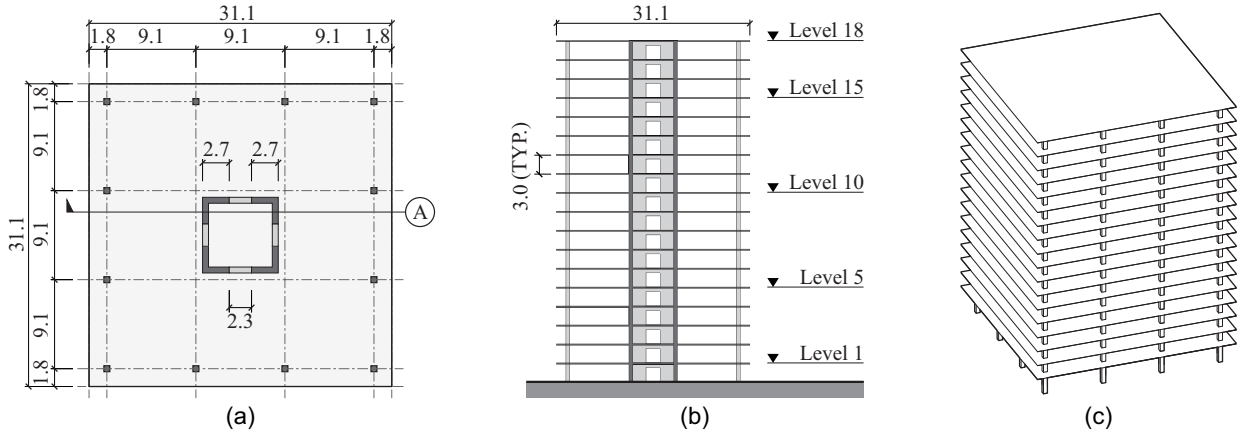


Fig. 3. (a) Typical floor plan; (b) section A; and (c) schematic of the 18-story core wall building. (All dimensions in meters.)

J. Struct. Eng., 2025, 151(2): 04024203

Downloaded from ascelibrary.org by University of California, San Diego on 12/17/24. Copyright ASCE. For personal use only; all rights reserved.

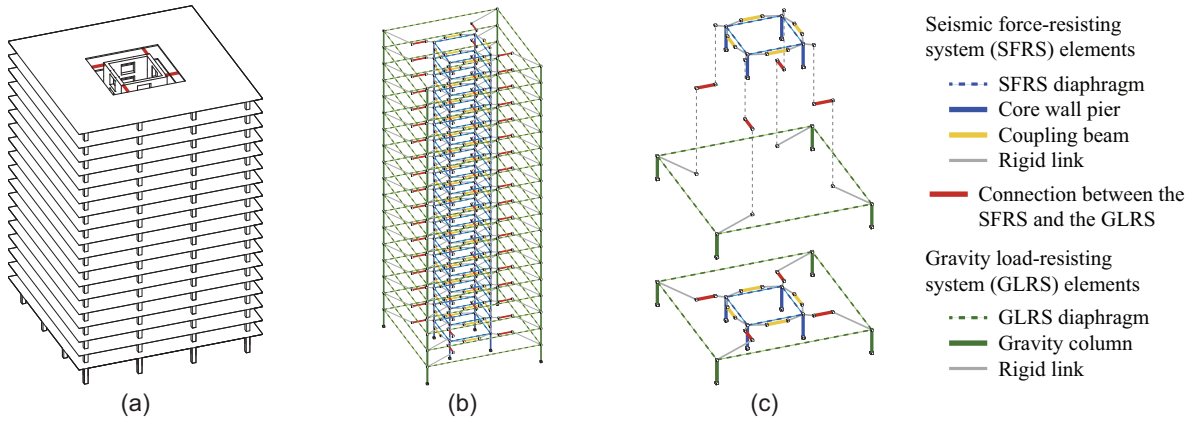


Fig. 4. (Color) (a) Schematic illustration; (b) OpenSees numerical model; and (c) elements in the typical story of the 18-story core wall building model.

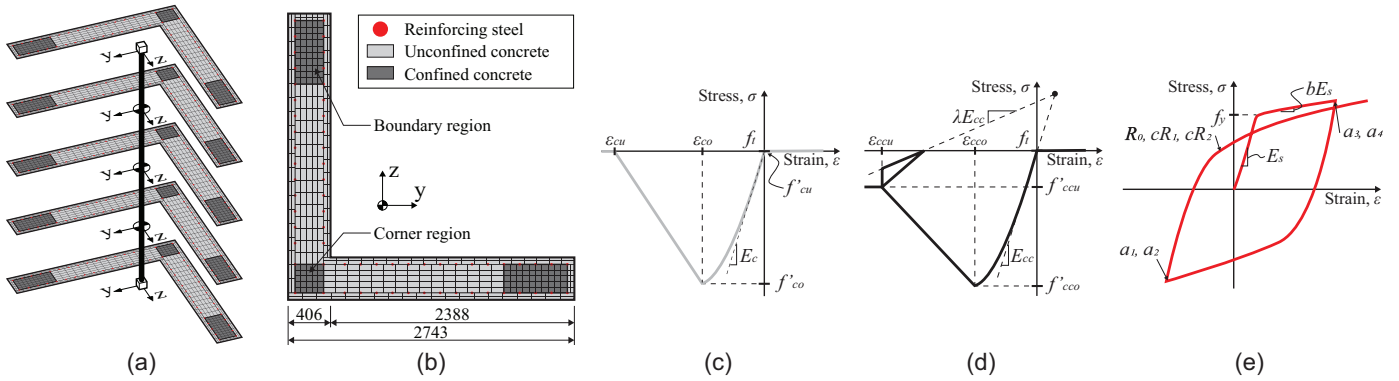


Fig. 5. (Color) (a) Typical wall pier element with fiber sections; (b) fiber section of the wall pier on floor Level 12 (all dimensions in millimeters); and material models simulating the stress-strain response of the (c) unconfined concrete; (d) confined concrete; and (e) reinforcing steel.

subjected to design-level earthquake ground motions and therefore were not simulated.

The stress-strain response of the unconfined and confined concrete in the core wall was simulated using the Concrete02 material model (Mohd Yassin 1994) in OpenSees, as shown in Figs. 5(c and d). The concrete model parameters were defined based on the selected nominal material properties and references available in the literature. More specifically, the unconfined concrete compressive strength at 28 days (f'_{co}) is −55 MPa (Tauberg et al. 2019), the unconfined concrete strain at the maximum strength (ε_{co}) is −0.002 (Kent and Park 1971), the unconfined concrete crushing strength (f'_{cu}) is 0 MPa (Tauberg et al. 2019), and the unconfined concrete strain at crushing strength considering the strain regularization addressing the numerical deformation localization issue (ε_{cu}) is −0.0046 (Coleman and Spacone 2001; Kent and Park 1971). The confined concrete material model parameters are shown in Table 1, which lists the confined concrete compressive strength at 28 days (f'_{cco}) (Mander et al. 1988), the confined concrete strain at the maximum strength (ε_{cco}) (Mander et al. 1988), the confined concrete crushing strength (f'_{ccu}) (Kent and Park 1971), and the confined concrete strain at crushing strength considering the strain regularization addressing the numerical deformation localization issue (ε_{ccu}) (Coleman and Spacone 2001; Moehle 2014) at the corner and boundary confined regions over the height of the building. Here, λ is the ratio of the reduced modulus of elasticity of concrete associated with the concrete strain at crushing strength (ε_{cu} for unconfined concrete and ε_{ccu} for confined concrete) to the initial modulus of elasticity of concrete (E_c for unconfined concrete and E_{cc} for confined concrete), and λ was set as 0.25 for both unconfined and confined concrete material models. Numerical convergence issues may occur if a nonzero value is used for the concrete tensile strength (f_t) in the Concrete02 material model. So, the f_t value was set to zero because the effect of the f_t value in the numerical simulation results was assessed to be negligible from a conducted sensitivity study.

Table 1. Confined concrete material model parameters

Confined region	f'_{cco} (MPa)	ε_{cco}	f'_{ccu} (MPa)	ε_{ccu}
Corner region				
1F–8F	69.64	−0.0046	13.93	−0.0253
9F–18F	73.98	−0.0054	14.80	−0.0313
Boundary region				
1F–8F	72.60	−0.0051	14.52	−0.0272
9F–18F	75.08	−0.0056	15.02	−0.0273

The stress-strain relationship of the longitudinal reinforcing steel in the wall piers was simulated using the SteelMPF material model (Menegotto and Pinto 1973; Filippou et al. 1983) in OpenSees, as shown in Fig. 5(e). The stress-strain relationship of the SteelMPF material model is governed by the following 10 parameters: yield strength (f_y), initial Young's modulus (E_s), strain hardening ratio (b), initial value of the curvature parameter (R_0),

Downloaded from ascelibrary.org by University of California, San Diego on 12/17/24. Copyright ASCE. For personal use only; all rights reserved.

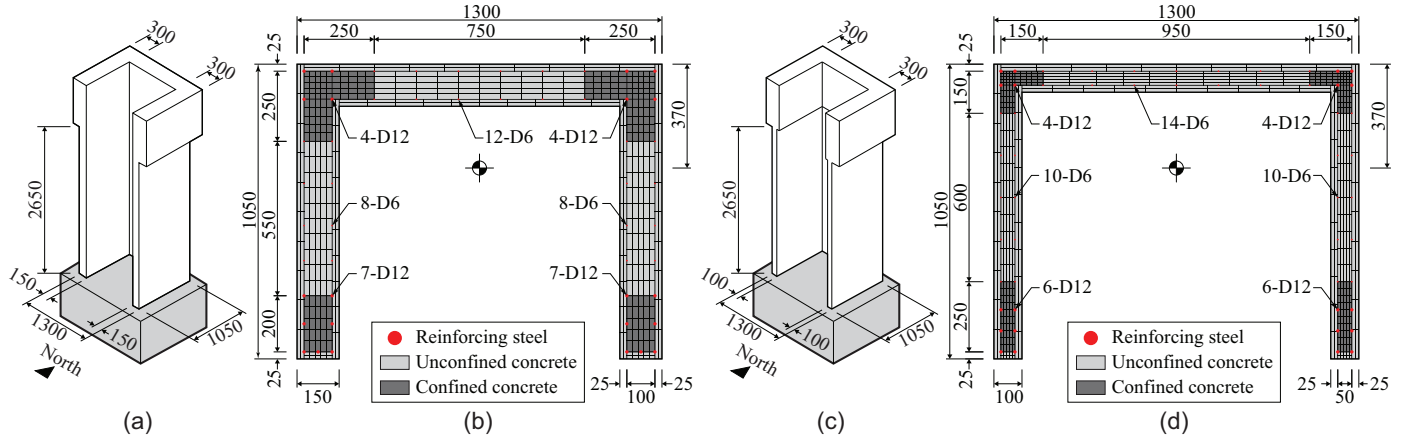


Fig. 6. (Color) Geometries of (a) TUA; and (c) TUB (Beyer et al. 2008); and fiber sections of (b) TUA; and (d) TUB. (All dimensions in mm.)

Table 2. Baseline values, standard deviations, and calibrated values for the SteelMPF material model parameters

Parameter	E_s (MPa)	b	R_0	cR_1	cR_2	a_1	a_3
Baseline value	29,969	0.02921	20	0.94660	0.09300	0.05075	0.02200
Standard deviation	—	0.00324	—	0.01778	0.02565	0.01092	0.00812
Calibrated value	29,969	0.02921	20	0.96000	0.07000	0.05075	0.02200

curvature degradation parameters (cR_1 and cR_2), and isotropic hardening components (a_1, a_2, a_3, and a_4). The elastic parameters (f_y and E_s) were quantified based on the nominal parameters of the selected material. The postyield parameters (b, R_0, cR_1, cR_2, a_1, a_2, a_3, and a_4) were quantified by calibration because no empirical equations are given in the literature for them (Birrell et al. 2021). The calibration of the wall pier numerical model was done at the component level using experimental test results adopted from Beyer et al. (2008), where quasi-static cyclic loading was applied to two types of U-shaped reinforced concrete wall specimens with different wall thicknesses, termed TUA and TUB, as shown in Figs. 6(a and c). During the experimental test, a constant axial load, accounting for the tributary area of a core wall in a typical 6-story building, was applied to the specimens by post-tensioning. In addition, a bidirectional displacement-controlled load was applied at the top of the specimens with displacement ductility levels of 1, 2, 3, 4, 6, and 8 until failure. Numerical models of the specimen TUA and TUB were generated in OpenSees using force-based nonlinear elements with fiber sections with concrete and steel material models, as shown in Figs. 6(b and d). The same displacement-controlled loading histories used in the experimental tests were applied to the corresponding numerical models.

Calibration was performed by altering the values for the five postyield parameters of the SteelMPF material model: b, cR_1, cR_2, a_1, and a_3. The values considered for calibration for each parameter were selected as baseline values adopted from Mayorga et al. (2022) and Mayorga and Tsampras (2024), with a range selected based on the standard deviation of each parameter presented by Birrell et al. (2021). One calibrated value for each parameter that best matched the stiffness of loading and unloading branches and the maximum force levels of the numerical model results with the experimental test results were determined. Table 2 shows the baseline value, standard deviation, and calibrated value for each parameter. Fig. 7 compares the experimental force-displacement response of TUA and TUB in east-west (EW) and north-south (NS) directions with the numerical force-displacement response of the simulated specimens considering the calibrated values of the SteelMPF material model parameters listed in Table 2. The results presented in Fig. 7 show that the responses from the numerical model match reasonably well with the responses from the experimental test.

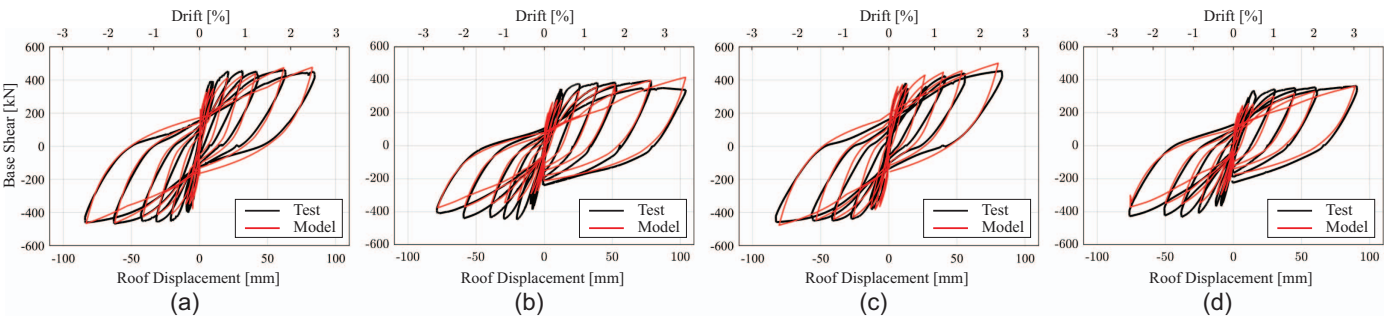


Fig. 7. (Color) Hysteretic response of TUA in (a) EW; and (b) NS directions; and hysteretic response of TUB in (c) EW; and (d) NS directions.

Downloaded from ascelibrary.org by University of California, San Diego on 12/17/24. Copyright ASCE. For personal use only; all rights reserved.

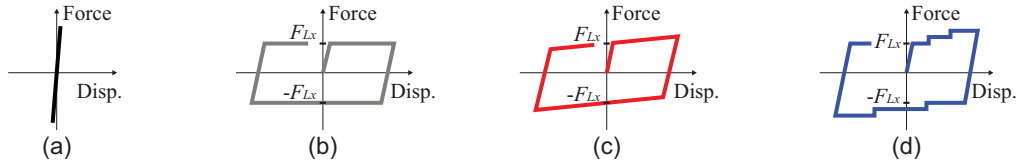


Fig. 8. (Color) Force-displacement relationship of four types of connections between the GLRS and SFRS: (a) RE = monolithic connection; (b) FD = force-limiting connection with constant limiting force; (c) FD+RB = force-limiting connection with linearly varying limiting force; and (d) Modified FD = force-limiting connection with predetermined discrete variable limiting force.

Downloaded from ascelibrary.org by University of California, San Diego on 12/17/24. Copyright ASCE. For personal use only; all rights reserved.

Modal Analysis and Damping Model

Modal analysis was performed to quantify the dynamic properties of the building model at its initial elastic state. The modal analysis results were used to compute the parameters required for the damping model. The fundamental mode is a torsional mode with a period of 3.18 s. The first translational modes in the global X- and Y-directions both have a period of 2.06 s. The second torsional mode has a period of 0.95 s, and the second translational modes in the global X- and Y-directions both have a period of 0.55 s. The core wall building model utilizes the Rayleigh damping model. The parameters of the Rayleigh damping model were determined by specifying the damping ratio to two periods of the structure, $0.2T_1$ and $1.5T_1$, in accordance with the National Earthquake Hazards Reduction Program (NEHRP) seismic design technical brief (Deierlein et al. 2010), where T_1 is the first translational mode period of the building model at its initial elastic state. The damping ratio was defined as 0.0268, according to Los Angeles Tall Buildings Structural Design Council (LATBSDC) alternative analysis and design procedure (LATBSDC 2020). The damping matrix was updated each time the tangent stiffness of the building model changed.

Connections between GLRS and SFRS

Types of Connections between GLRS and SFRS

Four types of connections are considered between the GLRS and SFRS of the core wall building model. The force-displacement relationships of the four types of connection are shown in Figs. 8(a–d). The first connection, the RE connection, represents the conventional monolithic connection between the GLRS and SFRS in core wall buildings. The comparison between the seismic response of the building model with the Modified FDs and the seismic response of the building model with the RE connections can assess the effectiveness of using the Modified FDs in limiting the magnitude and variability of the seismic response in core wall buildings compared to the conventional monolithic connections. The second connection, the FD, represents a force-limiting connection with a bilinear force-displacement response with zero postelastic stiffness. The FD represents a force-limiting connection with only a friction device and no rubber bearings. The results from the numerical simulations with the FDs can demonstrate the necessity for positive postelastic stiffness in preventing excessive connection deformation. The third connection, the FD+RB, represents a force-limiting connection with a bilinear force-displacement response with positive postelastic stiffness. The FD+RB represents the force-limiting connection with a friction device and rubber bearings developed for buildings with planar SFRS. The fourth connection, the Modified FD, is the force-limiting connection with predetermined discrete variable friction forces developed for buildings with core wall SFRS. Even though the FD+RB is physically and kinematically not compatible with buildings with core wall SFRS, it is considered in this study because the force-displacement response of the FD+RB improves the seismic performance of buildings with planar SFRS without excessive connection deformations. Thus, the comparison between the seismic response of the building model with the Modified FDs and the seismic response of the building model with the FD+RBs can identify if the predetermined discrete variable limiting force of the Modified FD can accomplish a similar seismic response of the building model as the linearly varying limiting force of the FD+RB.

Preliminary Design Force of Force-Limiting Connections

The three types of force-limiting connections (FD, FD+RB, and Modified FD) shown in Figs. 8(b–d), respectively, include the same F_{Lx} value in defining their force-displacement relationships, where F_{Lx} is the design limiting force at floor level x, that defines the transitions from linear elastic to postelastic force-displacement response in the force-limiting connections. The F_{Lx} is determined by the force-based method proposed by Tsampras and Sause (2022), and it can be used for the preliminary design of the force-limiting connections. The computation of F_{Lx} for $n \geq 3$ is shown in Eq. (1), where n is the total number of floor levels above the base of a structure; C_{Lx} is the design acceleration coefficient at floor level x; w_{px} is the seismic weight tributary to the diaphragm at floor level x; R_{DC} is the force-limiting connection design force factor that modifies the magnitude of F_{Lx}; and n_{Lx} is the number of force-limiting connections at floor level x that transfer forces along the horizontal translational direction of interest

$$F_{Lx} = \frac{C_{Lx}}{R_{DC}} \frac{w_{px}}{n_{Lx}} \tag{1}$$

The distribution of C_{Lx} and F_{Lx} over the height of a building is shown in Figs. 9(a and b), respectively. Here, h_1 is the height of floor Level 1; h_x is the height of floor level x; and h_n is the height of floor level n. Additionally, $F_{L1} = F_{L0}$ is the design limiting force at floor Level 1, and F_{Ln} is the design limiting force at floor level n. Fig. 9(c) shows a free-body diagram of an SFRS subjected to F_{Lx}, where V_{bFLx} and M_{bFLx} are the shear and moment at the base of the SFRS due to F_{Lx}, respectively. The value of F_{Lx} for one force-limiting connection at each floor level of the studied core wall building was calculated considering five different R_{DC} values, as shown in Fig. 9(d). A higher R_{DC} value results in smaller F_{Lx} values. Also, F_{Lx} is constant from floor Level 1 to floor Level 14, and increases from floor Level 14 to floor Level 18 to account for the second- and higher-mode effects. Tsampras and Sause (2022) recommended R_{DC} values for 12-, 8-, and 4-story reinforced concrete planar wall buildings with the FD+RBs. However, an estimate of R_{DC} for buildings with Modified FDs was not available; R_{DC} is one of the design parameters that is assessed through systematic parametric numerical earthquake simulations in the following section.

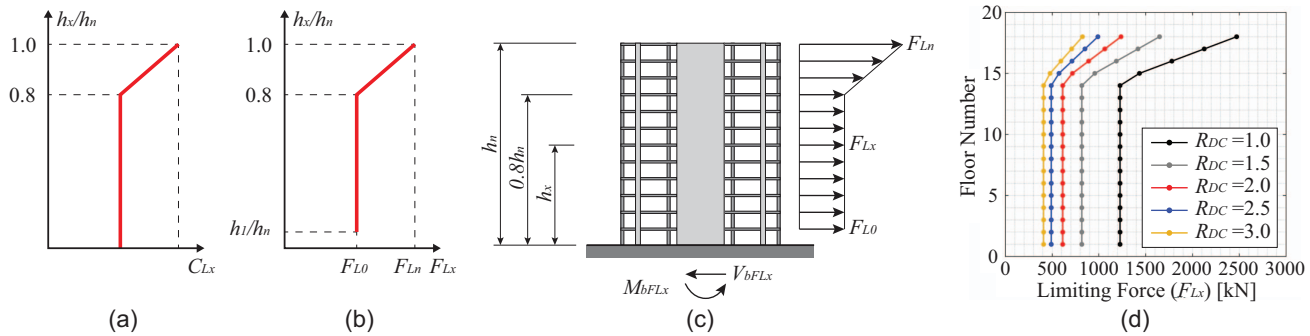


Fig. 9. (Color) Distribution of (a) C_{Lx}; and (b) F_{Lx} over the height of a building (Tsampras and Sause 2022); (c) free-body diagram of an SFRS subjected to F_{Lx} (Tsampras and Sause 2022); and (d) calculated F_{Lx} for one force-limiting connection at each floor level of the studied core wall building considering five R_{DC} values.

Modeling Approach of Force-Limiting Connections

The connections between the GLRS and SFRS were modeled using the corotational truss element in OpenSees. A corotational truss element restrains only the axial degree of freedom and releases all the remaining degrees of freedom at the two end nodes connected by the element. The force-displacement response of the RE connection was modeled using a stiffness that is orders of magnitude larger relative to the stiffness of other elements to simulate the high stiffness of a conventional monolithic connection. The force-displacement response of the force-limiting connections was modeled using the uniaxial material assigned to the corotational truss element as a normalized force-displacement response. The normalized force was calculated as the internal axial force of the truss element divided by the reference cross-sectional area of the truss element, termed A_{truss}, which is equal to 645 mm^2 (i.e., 1.0 in.^{2}). The normalized displacement was calculated as the internal axial deformation of the truss element divided by the reference length of the truss element, termed L_{truss}, which is equal to the total approximate length of the friction device.

The normalized force-displacement response of the FD, which is assumed to have a Coulomb type of friction force-displacement response (i.e., elastic-perfectly plastic), was defined using the Steel01 material model in OpenSees. The yield strength of the Steel01 was set equal to F_{Lx} normalized by A_{truss}. The modulus of elasticity of the Steel01 was set equal to K_{fr} normalized by A_{truss}/L_{truss}; and K_{fr} was set equal to 1,401 kN/mm, which represents the expected elastic stiffness of a force-limiting connection (Tsampras et al. 2017). The strain-hardening ratio of the Steel01 equal to 0.00001 simulates the zero postelastic stiffness of the friction device. The normalized force-displacement response of the FD +RB was defined using two uniaxial materials in parallel. The first uniaxial material was the Steel01 material model used in the FD, simulating the friction mechanism. The second uniaxial material was the linear elastic uniaxial material with the modulus of elasticity set equal to K_{RB} normalized by A_{truss}/L_{truss} to simulate the constant positive postelastic stiffness, where K_{RB} is the shear stiffness of rubber bearings with a value of 3.9 kN/mm (Tsampras et al. 2016b). The normalized force-displacement response of the Modified FD was defined utilizing the aggregate material model presented by Chen et al. (2023). The expected force-displacement response of the Modified FD is defined by the design parameters F_1, F_2, F_3, D_1, D_2, K_1, K_2, and K_3, as previously mentioned with Fig. 2(c). The F_1 was set equal to F_{Lx}. The design parameters that define the force-displacement response of the Modified FD were simplified to R_{DC}, D_1, D_2, F_2, and F_3.

Pareto Front Analysis to Determine Design Parameters of the Modified FD

Parametric numerical earthquake simulations were performed using a simplified 2D 18-story reinforced concrete planar wall building model to determine a set of the five design parameters of the Modified FD (R_{DC}, D_1, D_2, F_2, and F_3) that result in an improved seismic response of the building model. A simplified 2D 18-story building model instead of a 3D model was used to reduce the computational demand associated with the large number of numerical simulations conducted in this task. The range of values considered for the five design parameters of the Modified FD is listed in Table 3. One combination of values for the five design parameters is termed a sample. Out of 1,536 possible samples that can be created by the listed values for the five design parameters of the Modified FD, 1,031 samples were selected after eliminating unfeasible samples (e.g., D_1 cannot be larger than D_2) and samples with convergence issues due to excessive lateral displacement demand.

The simplified 2D 18-story building model consists of a reinforced concrete planar wall SFRS, a GLRS, and the Modified FDs connecting the two systems at every floor level. The reinforced concrete planar wall SFRS was modeled using force-based beam-column elements with fiber sections. The GLRS column was modeled using the elastic beam-column element with cracked section properties according to ACI 318-19 (ACI 2019). The Modified FD was modeled using the corotational truss element as described in the previous section on the modeling approach of force-limiting connections, using each sample of the five design parameters. The parametric numerical earthquake simulations of the simplified 2D 18-story building model utilized the 18 ground motions used by Tsampras and Sause (2022).

The parametric numerical earthquake simulation results corresponding to each sample were analyzed. Six representative design-related responses, termed objective responses, were selected to

Table 3. Values considered for the five design parameters of the Modified FD

R_{DC}	D_1 [mm (in.)]	D_2 [mm (in.)]	F_2	F_3
2.50	12.7 (0.5)	25.4 (1.0)	$0.125F_{Lx}$	$0.125F_{Lx}$
2.00	25.4 (1.0)	50.8 (2.0)	$0.250F_{Lx}$	$0.250F_{Lx}$
1.67	38.1 (1.5)	76.2 (3.0)	$0.375F_{Lx}$	$0.375F_{Lx}$
1.25	50.8 (2.0)	101.6 (4.0)	$0.500F_{Lx}$	$0.500F_{Lx}$
1.00	—	—	—	—
0.80	—	—	—	—

Downloaded from ascelibrary.org by University of California, San Diego on 12/17/24. Copyright ASCE. For personal use only; all rights reserved.

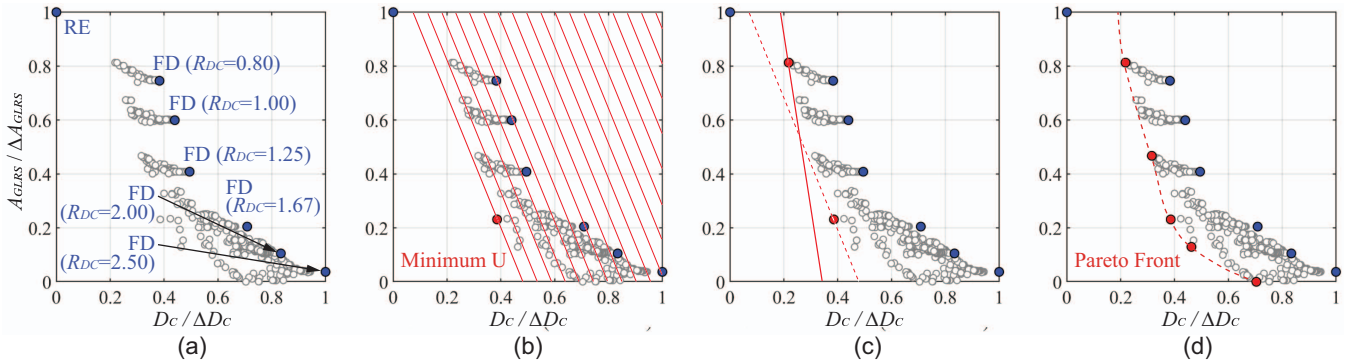


Fig. 10. (Color) Example process of determining the Pareto front for a multiobjective function with two objective functions.

determine the improved seismic responses of the simplified 2D 18-story building model. The six objective responses are the connection deformation, GLRS floor total acceleration, SFRS story shear, SFRS story moment, GLRS drift ratio, and SFRS wall base compressive strain responses. The maximum (over the height of the building model) of the mean (over 18 ground motions) of the peak (over the time history) value for each objective response was calculated for each sample. The list of the maximum mean peak values for an objective response, denoted as r_i (where i varies from 1 to 6 for the six objective responses), is as follows: $r_1 \equiv D_c$ represents the connection deformation response; $r_2 \equiv A_{GLRS}$ represents the GLRS floor total acceleration response; $r_3 \equiv V_{SFRS}$ represents the SFRS story shear response; $r_4 \equiv M_{SFRS}$ represents the SFRS story moment response; $r_5 \equiv \delta_{GLRS}$ represents the GLRS drift ratio response; and $r_6 \equiv \varepsilon_{SFRS}$ represents the SFRS wall base compressive strain response.

An improved seismic response of the simplified 2D 18-story building model can be represented as a simultaneous reduction of r_1, r_2, r_3, r_4, r_5, and r_6. Determining a set of samples that results in simultaneously minimized r_1, r_2, r_3, r_4, r_5, and r_6 is a multiobjective optimization problem, and it can be solved using the weighted sum method (Arora 2017). The multiobjective function U, shown in Eq. (2), is a superposition of the six objective functions $(r_i/\Delta r_i)$ multiplied by weights (w_i), where i varies from 1 to 6 for the six considered objective functions; and Δr_i represents the difference between the largest value and the smallest value in r_i [i.e., $\Delta r_i = \max(r_i)\text{-}\min(r_i)$]. By systematically altering the weights, a set of samples that minimize U can be determined. This set of samples is called the Pareto front

$$U = \sum_{i=1}^{6} w_i \frac{r_i}{\Delta r_i} \tag{2}$$

An example process of determining the Pareto front for a multiobjective function U with two objective functions, the normalized D_c (i.e., $D_c/\Delta D_c$) and the normalized A_{GLRS} (i.e., $A_{GLRS}/\Delta A_{GLRS}$), is presented in Eq. (3). Fig. 10(a) shows the two objective functions, where each white marker represents the numerical simulation results for the building model with the Modified FDs of each sample. The blue markers represent the numerical simulation results for the building model with the RE connections and the building models with the FDs. The normalized D_c and the normalized A_{GLRS} have an approximately inverse proportional relationship. Eq. (3) can be modified as Eq. (4) to represent a line with a slope of $(-w_1/w_2)$ and a y-intercept of (U/w_2). Thus, with a given w_1 and w_2, determining a Pareto front sample (i.e., a set of values for the normalized D_c and the normalized A_{GLRS} that results in minimum U) in Eq. (3) is equivalent to determining a line of Eq. (4) that intersects at least one white marker with the least y-intercept value, shown with a red marker in Fig. 10(b). With a different set of values for w_1 and w_2, another Pareto front sample can be determined, as shown in Fig. 10(c). By systematically altering the values for w_1 and w_2, the Pareto front was determined, as shown in Fig. 10(d)

$$U = \sum_{i=1}^{2} w_i \frac{r_i}{\Delta r_i} = w_1 \frac{D_c}{\Delta D_c} + w_2 \frac{A_{GLRS}}{\Delta A_{GLRS}} \tag{3}$$

$$\frac{A_{GLRS}}{\Delta A_{GLRS}} = \left(-\frac{w_1}{w_2}\right) \frac{D_c}{\Delta D_c} + \left(\frac{U}{w_2}\right) \tag{4}$$

The Pareto front of the multiobjective function U with six objective functions (normalized D_c, normalized A_{GLRS}, normalized V_{SFRS}, normalized M_{SFRS}, normalized δ_{GLRS}, and normalized ε_{SFRS}) was determined following the same method demonstrated with two objective functions in the previous paragraph. Fig. 11 shows the results in six-dimensional (6D) space utilizing five 2D projected views with each axis representing each objective function $(r_i/\Delta r_i)$ multiplied by Δr_i. Each white marker represents the numerical simulation results for the building model with the Modified FDs of each sample. The blue markers represent the numerical simulation results for the building model with the RE connections and the building models with the FDs. The red markers represent the determined Pareto front. It is observed that A_{GLRS}, V_{SFRS}, M_{SFRS}, and ε_{SFRS} are inversely proportional to D_c. The small variation range, less than 0.02, observed in the values of δ_{GLRS}, indicates that δ_{GLRS} is not sensitive to the variation of the five design parameters of the Modified FD. One Pareto front sample with the identification number 971 was arbitrarily selected out of 30 possible Pareto front samples to be used in the numerical earthquake simulations of the 3D 18-story core wall building model. The parameters of the selected Pareto front sample are $R_{DC} = 2.0$, $D_1 = 12.7$ mm, $D_2 = 25.4$ mm, $F_2 = 0.375F_{Lx}$, and $F_3 = 0.5\,F_{Lx}$. These parameters can be physically achieved by applying the design variations of the Modified FD presented by Chen et al. (2023).

Numerical Earthquake Simulations

Earthquake Ground Motions

Thirteen bidirectional far-field earthquake ground motions from the set of ground motions provided in FEMA P695 (FEMA 2009) were selected as the input excitation for the numerical earthquake

Downloaded from ascelibrary.org by University of California, San Diego on 12/17/24. Copyright ASCE. For personal use only; all rights reserved.

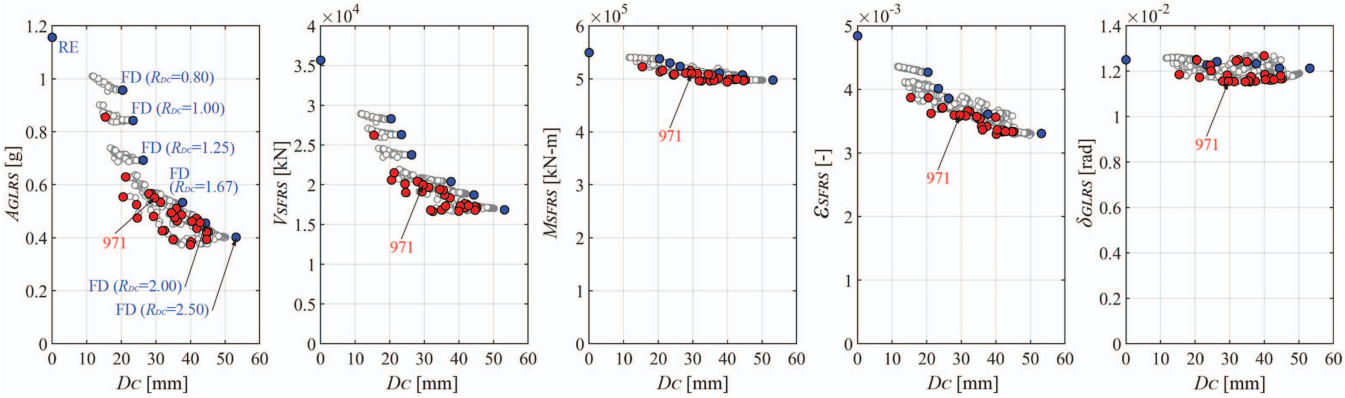


Fig. 11. (Color) Plots of the maximum mean peak values of the six objective responses (i.e., r_1, r_2, r_3, r_4, r_5, and r_6) for the building model with the Modified FDs used in the Pareto front analysis. The red markers indicate the Pareto front. The blue markers represent the maximum mean peak values of the six objective responses for the building model with the RE connections and the building models with the FDs.

Table 4. Thirteen far-field ground motions from FEMA P695

Earthquake number	Earthquake name	Recording station name	First orthogonal horizontal component, H_1	Second orthogonal horizontal component, H_2	Scale factor
EQ3	Imperial Valley	Delta	H-DLT262	H-DLT352	1.59
EQ4	Imperial Valley	El Century Array #11	H-E11140	H-E11230	1.78
EQ5	Superstition Hills	El Centro Imp. Co.	B-ICC000	B-ICC090	1.53
EQ6	Superstition Hills	Poe Road (temp)	B-POE270	B-POE360	1.73
EQ8	Loma Prieta	Gilroy Array #3	G03000	G03090	1.61
EQ11	Landers	Yermo Fire Station	YER270	YER360	1.76
EQ13	Northridge	Canyon Country-WLC	LOS000	LOS270	1.26
EQ15	Kobe, Japan	Shin-Osaka	SHI000	SHI090	1.87
EQ17	Kocaeli, Turkey	Duzce	DZC180	DZC270	1.13
EQ18	Chi-Chi, Taiwan	CHY101	CHY101-E	CHY101-N	0.87
EQ19	Chi-Chi, Taiwan	TCU045	TCU045-E	TCU045-N	1.68
EQ20	Duzce, Turkey	Bolu	BOL000	BOL090	0.94
EQ22	Hector Mine	Hector	HEC000	HEC090	1.68

Source: Data from FEMA P695 (FEMA 2009).

simulations of the 3D 18-story core wall building model, and they are listed in Table 4. The two orthogonal horizontal components of acceleration for each ground motion are termed H_1 and H_2. RotD50 response spectrum (Boore 2010), which accounts for the various horizontal orientations of a ground motion, was calculated for each ground motion, assuming a 5% damping ratio. Each ground motion was scaled so that the values of the RotD50 response spectra are reasonably close to the values of the target response spectrum over a period ranging from 0.41 to 4.12 s (Baker 2011). The target response spectrum is the design response spectrum calculated in accordance with ASCE 7-16 (ASCE 2016). The determined scale factor for each ground motion is listed in Table 4. Note that 40 s of zero acceleration were appended to the scaled ground motions time histories (i.e., zero-padded) to allow the computation of postearthquake residual responses of the building model. The scaled zero-padded H_1 and H_2 of each ground motion were applied at the base of the building model along the global translational X- and Y-directions, respectively.

Analysis Results

Numerical earthquake simulations of the 18-story core wall building model, described in the section "Numerical Model of the 18-Story Core Wall Building," were performed considering four different analysis cases. Each analysis case used the 18-story core wall building model with one of the four types of connections between the GLRS and SFRS discussed in the section "Connections between GLRS and SFRS." The analysis cases are termed the RE analysis case, the FD analysis case, the FD+RB analysis case, and the Modified FD analysis case, following the terminology of each connection. In this study, the design of the 18-story core wall building model remains the same for the four analysis cases because the use of the force-limiting connections does not aim to change the flexural design of the core wall. Instead, the use of the force-limiting connections aims to modify the shear-dominant higher-mode seismic responses. In addition, maintaining the same flexural design for the wall piers allows for a direct comparison between the four analysis cases.

Structural seismic responses of the 18-story core wall building model are shown in Fig. 12. The figure shows the peak floor total acceleration, SFRS story shear, SFRS story torsion, SFRS story drift ratio at the center of the slab inside the core, GLRS story drift ratio at the corner edge of the slab outside of the core, GLRS story torsional drift ratio, and connection deformation responses. The horizontal axis shows either the floor level or the story level. Each marker on the figure represents the peak (i.e., maximum absolute) value from the time-history response and the maximum value from the global translational X- and Y-direction responses. The color of

Downloaded from ascelibrary.org by University of California, San Diego on 12/17/24. Copyright ASCE. For personal use only; all rights reserved.

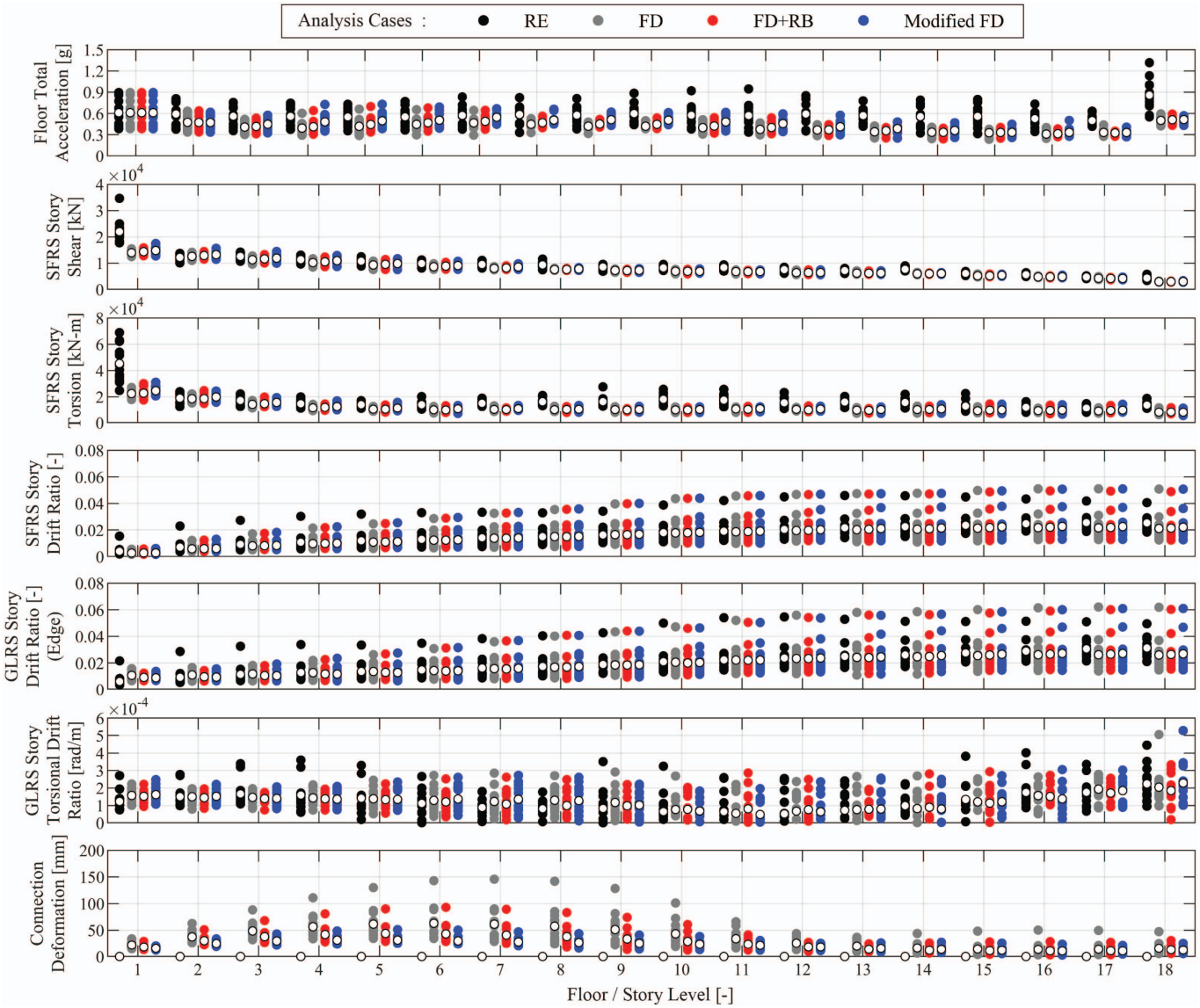


Fig. 12. (Color) Peak responses from numerical earthquake simulations of the four analysis cases.

the marker indicates the different analysis cases. The 13 markers at each floor level or story level for each analysis case indicate results from the 13 ground motions. The mean value of the peak responses from the 13 ground motions (termed the mean value of responses) is shown with a white marker.

The use of the force-limiting connections (FD, FD+RB, and Modified FD) reduced the magnitude and variability in the peak floor total acceleration response compared to the RE analysis case. The largest peak floor total acceleration response of the RE analysis case was obtained at the roof. The mean value of the peak floor total acceleration response at the roof was reduced by 42%, 40%, and 40% using the FDs, FD+RBs, and Modified FDs, respectively, compared to the RE analysis case. In addition, the standard deviation of the peak floor total acceleration response at the roof was reduced by 76%, 81%, and 77% using the FDs, FD+RBs, and Modified FDs, respectively, compared to the RE analysis case.

The use of the force-limiting connections reduced the magnitude and variability in the peak SFRS base shear response compared to the RE analysis case. The largest SFRS story shear response of the RE analysis case was obtained at the base. The mean value of the peak SFRS base shear response was reduced by 36%, 35%, and 33% using the FDs, FD+RBs, and Modified FDs, respectively, compared to the RE analysis case. In addition, the standard deviation of the peak SFRS base shear response was reduced by 79%, 76%, and 68% using the FDs, FD+RBs, and Modified FDs, respectively, compared to the RE analysis case.

The SFRS story torsional moment response was calculated as the sum of the torsional moment in all the wall pier elements and the moment created by the forces in all the wall pier elements. The use of the force-limiting connections reduced the magnitude and variability in the peak SFRS story torsional moment response at most story levels, compared to the RE analysis case. The mean value of the peak SFRS story torsional moment response at the base was reduced by 51%, 50%, and 46% using the FDs, FD+RBs, and Modified FDs, respectively, compared to the RE analysis case. In addition, the standard deviation of the peak SFRS story torsional moment response at the base was reduced by 80%, 75%, and 76% using the FDs, FD+RBs, and Modified FDs, respectively, compared to the RE analysis case.

The SFRS story drift ratio response was calculated at the center of the slab inside the core, and the GLRS story drift ratio response was calculated at the corner edge of the slab to consider the

Downloaded from ascelibrary.org by University of California, San Diego on 12/17/24. Copyright ASCE. For personal use only; all rights reserved.

maximum story drift accounting for the torsional response. Overall, the peak SFRS story drift ratio response, the peak GLRS story drift ratio response, and the peak GLRS story torsional drift ratio response using the force-limiting connections were similar to those from the RE analysis case. The increase in the peak SFRS and GLRS story drift ratio responses along the height of the building model is primarily attributed to the first mode responses of the building model. The use of the force-limiting connections reduced the mean value of the peak SFRS story drift ratio response near the roof, compared to the RE analysis case. The use of the force-limiting connections reduced the mean value of the peak GLRS story drift ratio response near the roof and increased the mean value of the peak GLRS story drift ratio response near the base, compared to the RE analysis case.

The connection deformation response was calculated as the maximum peak value of the four force-limiting connection deformation responses at each floor level. The mean value of the peak connection deformation response from the RE analysis case was practically zero at all floor levels because the RE connection was intended to simulate the conventional monolithic connection with high stiffness. The mean value of the peak connection deformation response was the largest from the FD analysis case due to the zero postelastic stiffness of the FD, demonstrating the necessity of postelastic stiffness to prevent excessive connection deformation. The mean value of the peak connection deformation response from the Modified FD analysis case was smaller than or similar to that from the FD+RB analysis case. This indicates that the discrete variable limiting force of the Modified FD resulted in a reasonable connection deformation response similar to the connection deformation response resulted from the linearly varying limiting force of the FD+RB. In addition, the standard deviation of the peak connection deformation was reduced from the FD+RB and Modified FD analysis cases, compared to the FD analysis case. This indicates that the presence of postelastic stiffness reduced the magnitude and variability of the connection deformation response. Furthermore, the distribution of the connection deformation over the height of the building model resembled a deformation shape dominated by the second and higher modes, with the largest connection deformation occurring at approximately 40% of the total height of the building. The uniformly distributed connection deformation demands near the roof were attributed to the increasing F_{Lx} values at floor levels from 14 to 18, as shown in Fig. 9. The contribution of the higher-mode responses to the total dynamic response of the building model is explained in the following subsection on reduction of higher-mode effects.

The residual drift ratios of the SFRS and GLRS from the four analysis cases are shown in Fig. 13, where each marker represents the peak (i.e., maximum absolute) value from the time-history response and the maximum value from the global translational *X*- and *Y*-direction responses. The 13 markers at each story level for each analysis case indicate results from the 13 ground motions. Earthquake 18 (EQ18) resulted in the largest residual drift ratio demand because the spectral displacement computed at the first translational mode period of the building model for EQ18 was higher than

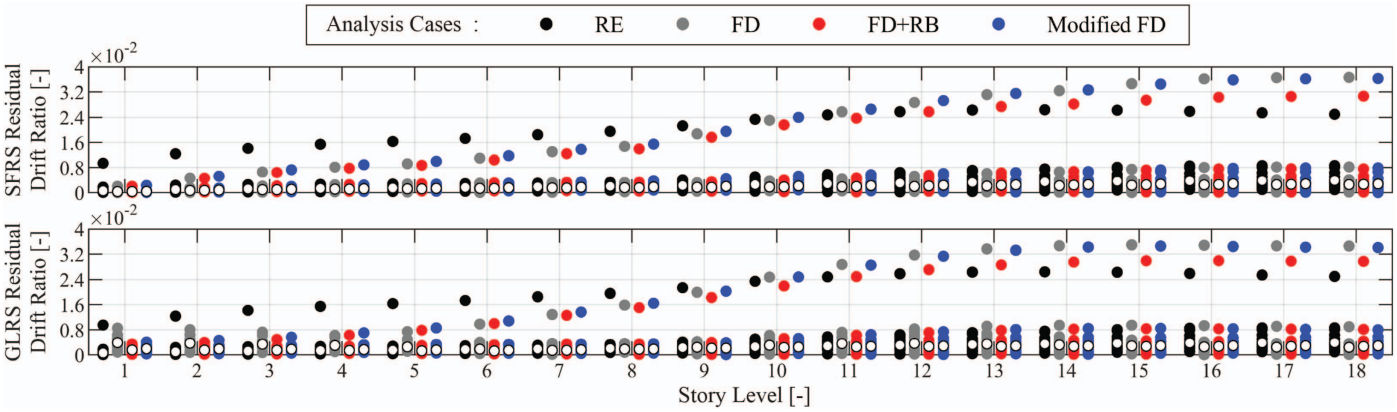


Fig. 13. (Color) Residual drift ratio of the SFRS and GLRS.

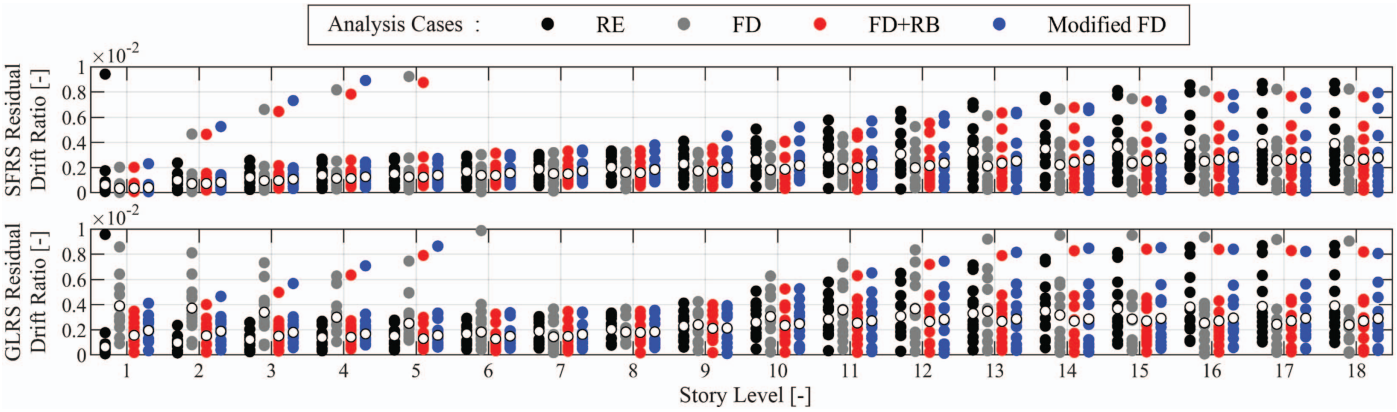


Fig. 14. (Color) Residual drift ratio of the SFRS and GLRS, focusing on the *y*-axis values within a range of [0, 0.01].

Downloaded from ascelibrary.org by University of California, San Diego on 12/17/24. Copyright ASCE. For personal use only; all rights reserved.

the spectral displacement computed at the first translational mode period of the building model for the remaining ground motions. The mean value of the peak responses from the 12 ground motions (not considering the outlier responses from EQ18) is shown with a white marker. The peak responses from EQ18 were excluded to limit the influence of the outlying response from the EQ18 ground motion. Fig. 14 shows the same information as Fig. 13, but focuses on the *y*-axis values within a range of [0, 0.01]. The use of the force-limiting connections resulted in reduced mean SFRS residual drift ratio compared to the RE analysis cases. The use of the force-limiting connections resulted in reduced mean GLRS residual drift ratio near the roof and increased mean GLRS residual drift ratio near the base compared to the RE analysis case. The maximum mean GLRS residual drift ratio was similar for the RE, FD, FD+RB, and Modified FD analysis cases.

The maximum and minimum strain responses at the wall base from the four analysis cases are shown in Figs. 15(a and b), respectively, where the maximum positive strain response values indicate tension and the minimum negative strain response values indicate compression. Fig. 15(c) shows the same information as Fig. 15(b), but focuses on the *y*-axis values within a range of [−0.01, 0]. The 13 markers indicate results from the 13 ground motions. The mean value of the results from the 12 ground motions (not considering the outlier responses from EQ18) is shown with a white marker. The results from EQ18 were excluded to limit the influence of the outlying response from the EQ18 ground motion. The use of the force-limiting connections reduced the magnitude and variability in the absolute values of the maximum and minimum strain responses at the wall base compared to the RE analysis case. The mean values of the absolute values of the maximum and minimum strain responses at the wall base were reduced by 41% and 37% on average, respectively, compared to the RE analysis case. In addition, the standard deviations of the absolute values of the maximum and minimum strain responses at the wall base were reduced by 55% and 62% on average, respectively, compared to the RE analysis case. Fig. 16 shows the distribution of the strain demand at the base section of the wall piers at the time of the maximum strain subjected to EQ18. EQ18 resulted in the largest maximum strain demands compared to other ground motions from all four analysis cases. The use of the Modified FD resulted in a more uniform distribution of strain demand at the wall base with reduced magnitude compared to the RE analysis case.

The strain time history and the stress-strain response at the wall base of the building model subjected to EQ18 are shown in Fig. 17. Figs. 17(a and b) show the strain time history of a steel fiber at which the RE and Modified FD analysis cases resulted in the maximum strain, respectively, and Figs. 17(c and d) show the corresponding stress-strain response, respectively. Figs. 17(e and f) show the strain time history of a confined concrete fiber at which the RE and Modified FD analysis cases resulted in the minimum strain, respectively, and Figs. 17(g and h) show the corresponding stress-strain response, respectively. Both the RE and Modified FD analysis cases experienced their peak strain at around 40 s in the time history. In the RE analysis case, the reinforcing steel and confined concrete fibers underwent an impulsive strain demand with maximum and minimum values of approximately 0.06 and −0.06, respectively, which resulted in similar magnitude residual strains. The minimum strain passed the confined concrete strain at crushing strength within a single cycle. Conversely, the Modified FD analysis case showed more reasonable strain demands, with peak strains below 2% and residual strains under 1% for the reinforcing steel fiber. The confined concrete fiber remained in the elastic range.

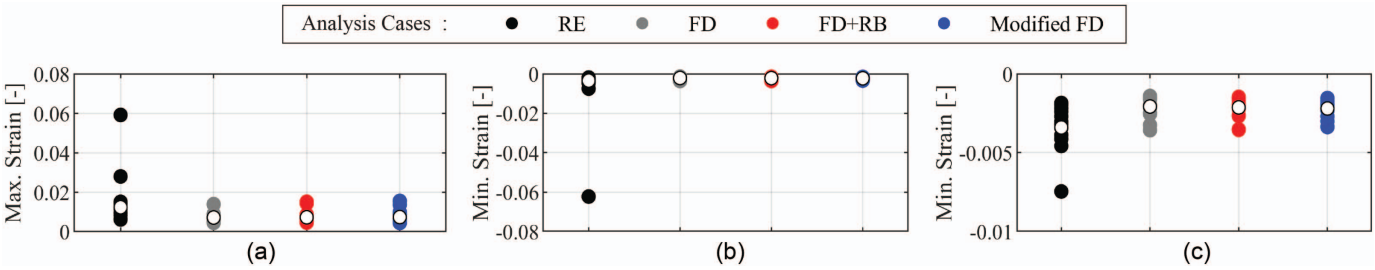


Fig. 15. (Color) Maximum and minimum strain responses at the wall base.

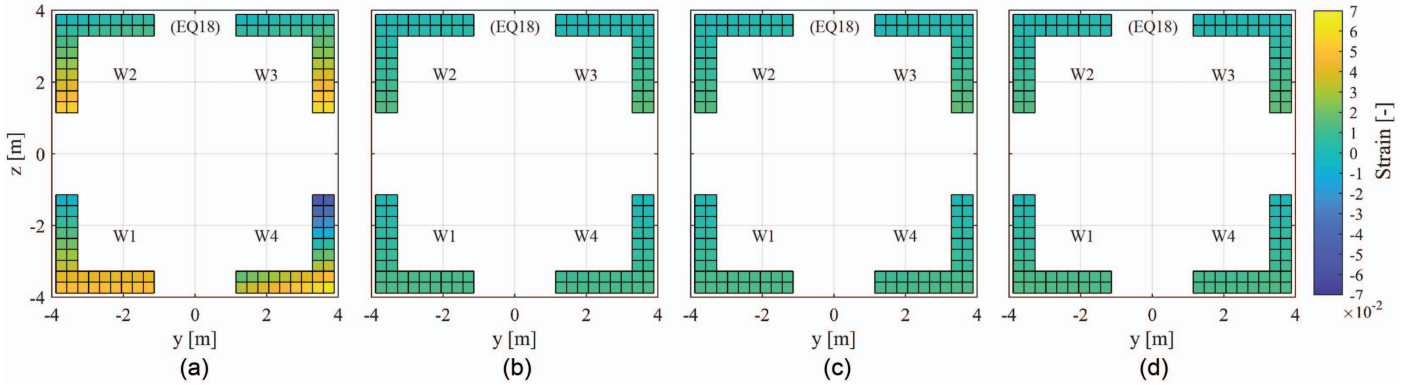


Fig. 16. (Color) Fiber section strain distribution at the wall base of the building model subjected to EQ18: (a) RE; (b) FD; (c) FD+RB; and (d) Modified FD.

Downloaded from ascelibrary.org by University of California, San Diego on 12/17/24. Copyright ASCE. For personal use only; all rights reserved.

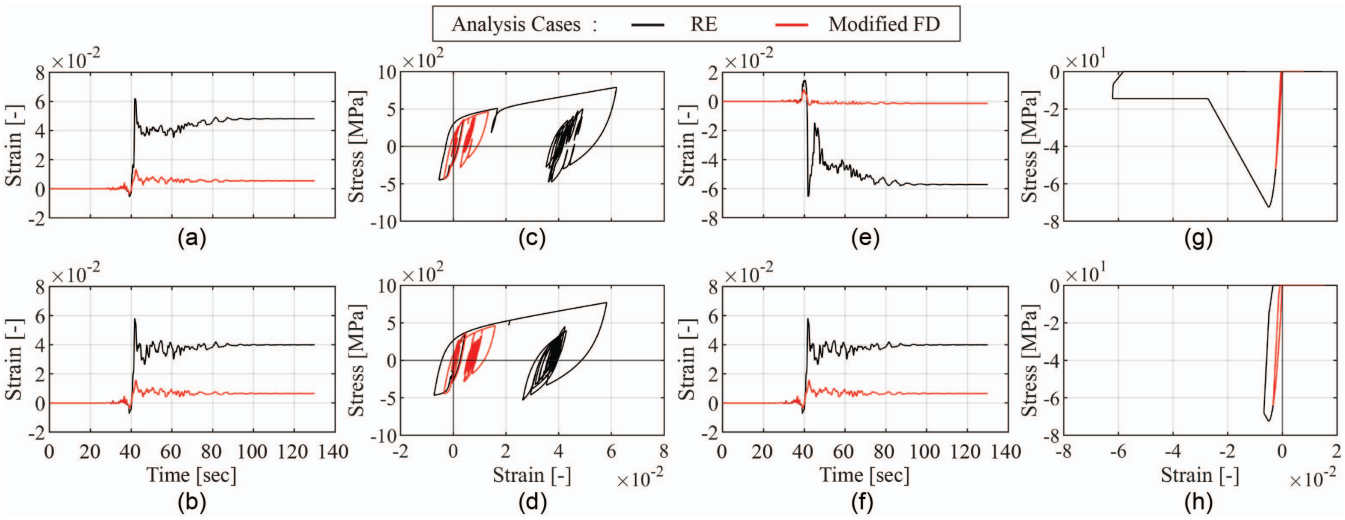


Fig. 17. (Color) Strain time history and stress-strain response at the wall base of the building model subjected to EQ18.

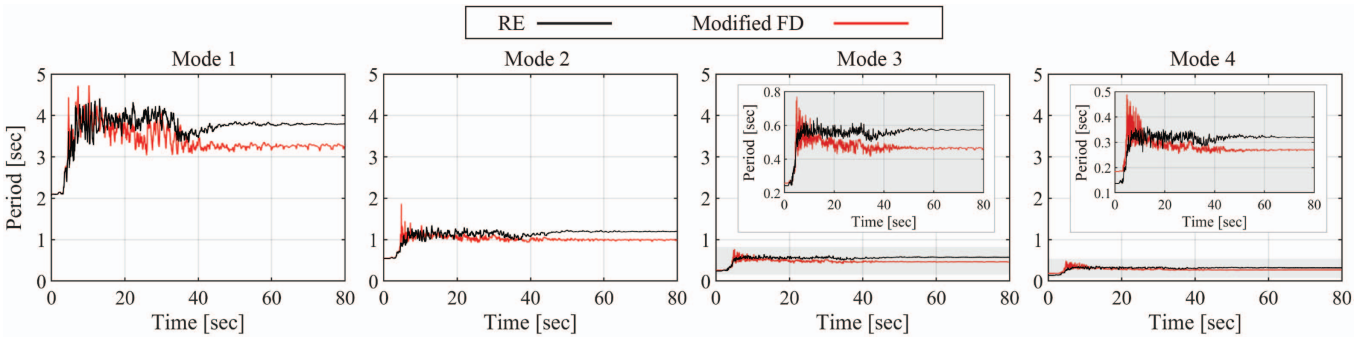


Fig. 18. (Color) Modal period time history in the global translational *X*-direction of the building model subjected to EQ8.

The reduction of strain demand at the wall base indicates a potential reduction in the expected structural damage in the wall piers, and can lead to a relaxation of special reinforcing detailing of the walls.

Reduction of Higher-Mode Effects

The reduction in the force and acceleration demands of the building model with the Modified FDs compared to the building model with the RE connections, as observed in the previous section, is related to the reduction of the seismic-induced responses associated with higher modes. This section demonstrates that the controlled inelastic response of the Modified FDs changes the instantaneous state of stiffness of the structural system and limits the magnitude and variability in the shear-dominant higher-mode-induced acceleration and force seismic responses.

The evolution of modal periods of the building model during the numerical earthquake simulation demonstrates that the use of the Modified FDs changed the instantaneous state of stiffness of the structural system. Fig. 18 shows the time history of the modal period in the global translational *X*-direction of the building model subjected to EQ8 in Table 4. EQ8 is the ground motion that resulted in the largest peak floor total acceleration response. The modal periods in the global translational *X*-direction were determined based on the modal participation mass ratios in the global translational *X*-direction considering the instantaneous tangent stiffness of the building model after the strong ground motion. The largest elongation in the modal periods, near 3 s in the time history, was related to the cracking of the concrete in the wall piers and the coupling beams. Moreover, the second-, third-, and fourth-mode periods of the Modified FD analysis case fluctuated within a larger range of modal periods with larger highest modal periods at the time of the peak excitation near 5 s in the time history, compared to the RE analysis case. The large fluctuation of the modal periods of the Modified FD analysis case implies that the instantaneous state of stiffness of the structural system was changed by the controlled inelastic response of the Modified FD. The modal period ranges of the Modified FD analysis case after the largest period elongation are 3.04~4.73 s, 0.93~1.86 s, 0.42~0.77 s, and 0.25~0.49 s for the first, second, third, and fourth translational modes, respectively. The damping ratios associated with the elongated modal period of the first, second, third, and fourth modes fell within a reasonable range. In addition, the smaller residual modal period of the Modified FD analysis case compared to the RE analysis case could indicate less structural damage accumulated with the use of the Modified FDs during the numerical earthquake ground motion.

Fig. 19 illustrates that the use of the Modified FDs reduced the magnitude of the higher-mode-induced floor total acceleration responses. Figs. 19(a–c) show the time history of the ground motion acceleration EQ8, H_1, and the time history of the roof total acceleration response in the global translational *X*-direction excited by EQ8 from the RE and Modified FD analysis cases, respectively.

Downloaded from ascelibrary.org by University of California, San Diego on 12/17/24. Copyright ASCE. For personal use only; all rights reserved.

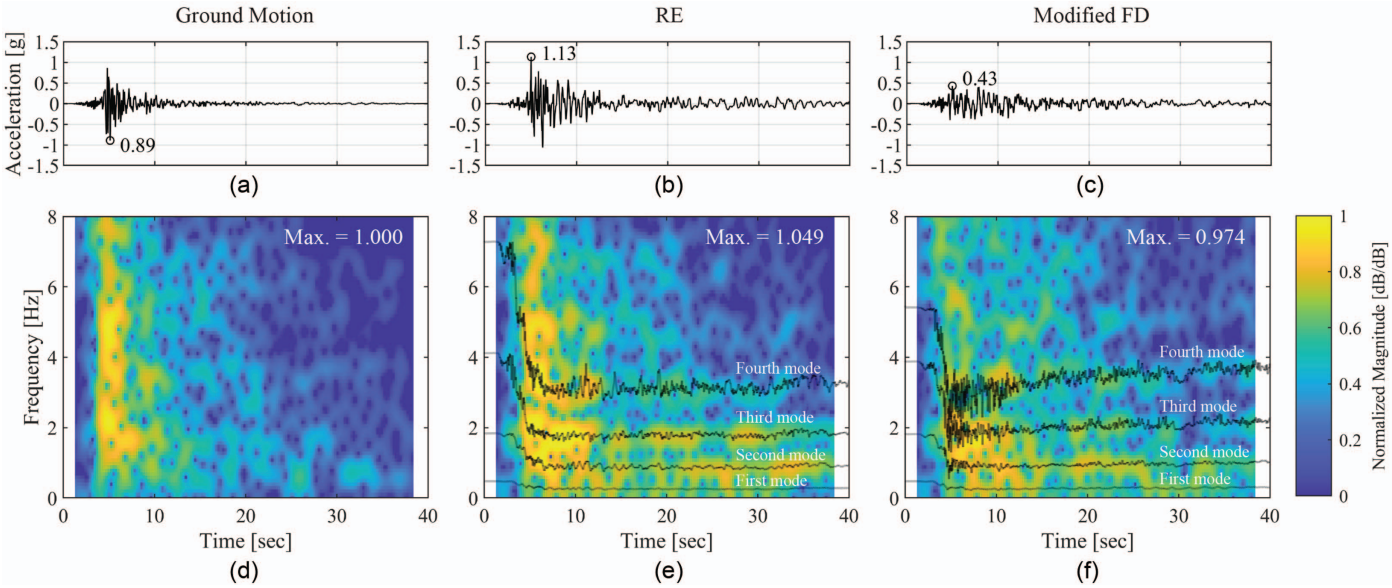


Fig. 19. (Color) (a) Time history of the ground motion acceleration EQ8, H_1; time history of the roof total acceleration response in the global translational X-direction excited by EQ8 from (b) the RE and (c) the Modified FD analysis cases; (d) spectrogram of the ground motion EQ8, H_1; and spectrogram of the roof total acceleration response in the global translational X-direction excited by EQ8 from (e) the RE and (f) the Modified FD analysis cases and the corresponding evolution of the first- through fourth-mode frequencies.

The peak roof total acceleration response from the RE analysis case was larger compared to the peak ground motion acceleration, indicating amplification of the ground motion excitation. Conversely, the peak roof total response from the Modified FD was smaller compared to the peak roof total acceleration response from the RE analysis case and the peak ground motion acceleration, indicating deamplification of the ground motion excitation. Fig. 19(d) shows the spectrogram of the time history of the ground motion acceleration EQ8, H_1, normalized by its peak power magnitude. Figs. 19(e and f) show the spectrograms of the time history of the roof total acceleration response in the global translational X-direction excited by EQ8 from the RE and Modified FD analysis cases, respectively, normalized by the peak power magnitude of the spectrogram of the ground motion acceleration EQ8, H_1. The modal frequency time histories from the RE and Modified FD analysis cases, equivalent to the modal period time histories shown in Fig. 18, are plotted over the spectrograms of the roof total accelerations. By overlaying the graphs, it is possible to associate specific translational modes with the time regions in the spectrogram where greater than 0.9 normalized magnitudes were observed. The spectrogram of the roof total acceleration for the RE analysis case indicated greater than 0.9 normalized magnitude in the second-, third-, and fourth-mode frequencies between 5 and 10 s of the time history. The spectrogram of the roof total acceleration for the Modified FD analysis case, compared to the RE analysis case, showed a reduction in the normalized magnitude in the second-, third-, and fourth-mode frequencies between 5 and 10 s of the time history. Moreover, the duration of the greater than 0.9 normalized magnitude in the second-, third-, and fourth-mode frequencies was reduced for the Modified FD analysis case compared to the RE analysis case.

Fig. 20(a) shows the pseudo-acceleration response spectra computed using the 13 ground motions in the global translational X-direction, termed SA_{gm}, presented as 13 thin lines. Figs. 20(b and c) show the pseudo-acceleration response spectra computed using the corresponding roof total acceleration response in the global translational X-direction, termed SA_{roof}, from the RE and the Modified FD analysis cases, respectively, presented as 13 thin lines. The computation of the response spectra considered a 5% damping ratio. The solid and dashed lines in Figs. 20(a–c) represent the mean values (Mean) and the mean values plus/minus one standard deviation (STD) of the 13 response spectra calculated at each period, respectively. The maximum standard deviations over the periods of the pseudo-acceleration response spectra from the

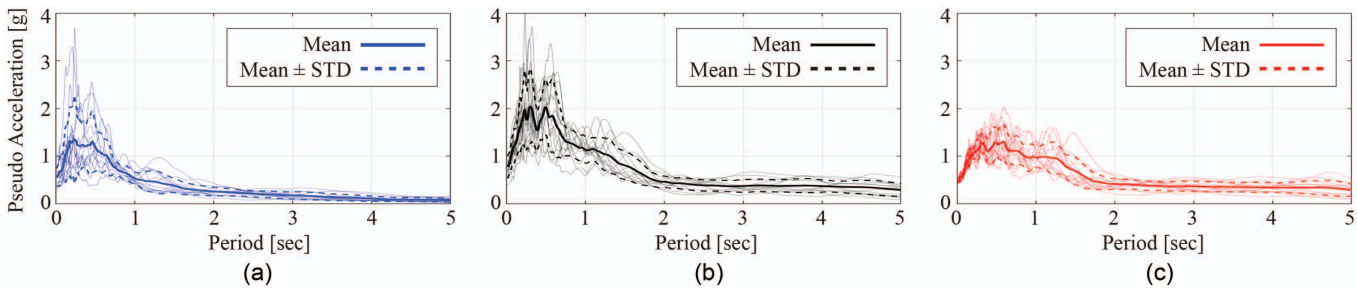


Fig. 20. (Color) Pseudo-acceleration response spectra computed from (a) the 13 ground motions; and corresponding roof total acceleration response from (b) the RE analysis case; and (c) the Modified FD analysis case.

Downloaded from ascelibrary.org by University of California, San Diego on 12/17/24. Copyright ASCE. For personal use only; all rights reserved.

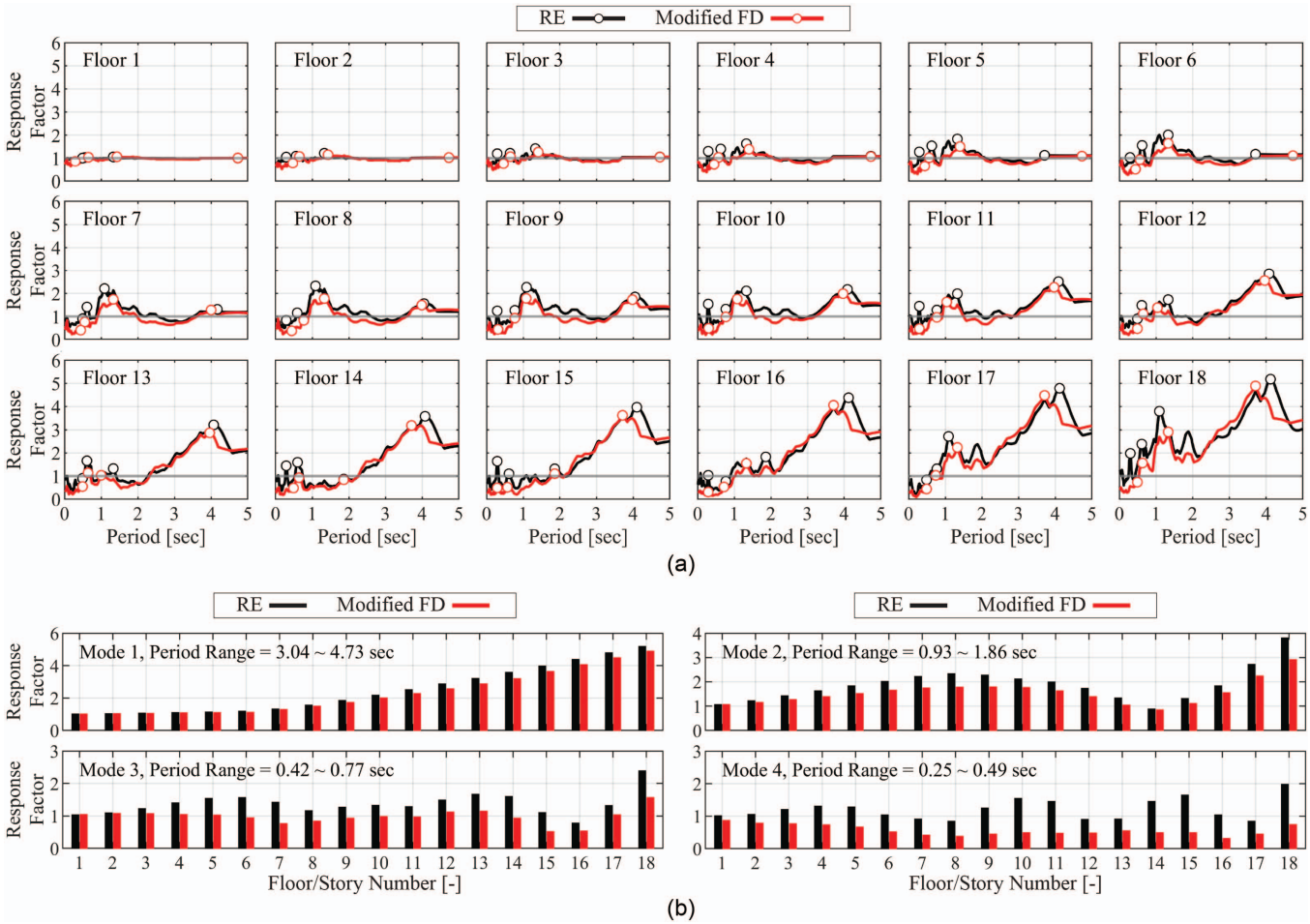


Fig. 21. (Color) (a) Pseudo-acceleration response factor spectra; and (b) peak pseudo-acceleration response factor of the first, second, third, and fourth modes of the building model subjected to EQ8.

ground motions, the RE analysis case, and the Modified FD analysis case were $0.9261g$, $0.8247g$, and $0.3689g$, respectively. The mean value of the 13 SA_{roof} from the Modified FD analysis case was reduced with significantly less variability in the higher-mode period range (approximately from 0 to 2 s) compared to the 13 SA_{roof} from the RE analysis case. This reduction of the magnitude and variability of SA_{roof} in the higher-mode period range was due to the controlled inelastic response of the Modified FDs that limits the forces transferred between the GLRS and the SFRS of the building model, thus limiting the total acceleration response.

The effect of Modified FDs is further assessed by analyzing the floor total acceleration response over the height of the building. The pseudo-acceleration response spectrum computed from the floor total acceleration response at floor level x, termed $SA_{floor,x}$, was calculated using the global translational X-direction floor total acceleration response at floor Levels 1 to 18 for both the RE and Modified FD analysis cases subjected to EQ8. The values of $SA_{floor,x}$ were normalized at every given period by SA_{gm} calculated using the ground motion acceleration EQ8, H_1. The result is a pseudo-acceleration response factor spectrum (i.e., $SA_{floor,x}/SA_{gm}$), shown in Fig. 21(a). The pseudo-acceleration response factor spectrum of each analysis case on each floor level has four peaks identified with white circular markers. The four peaks represent the maximum value within the modal period range for the first, second, third, and fourth modes, identified in Fig. 18. The peak values of the pseudo-acceleration response factor spectra over the height of the building model grouped by the modal period range are shown in Fig. 21(b). The variation of the peak pseudo-acceleration response factors over the height of the building model from the RE analysis case resembled the translational mode shapes expected from the linear elastic model of the studied building. The peak pseudo-acceleration response factors of each mode were reduced with the use of the Modified FDs compared to the RE analysis case, with the largest reduction ratio in the fourth-mode period range compared to the first-, second-, and third-mode period ranges. The reduction of the pseudo-acceleration response factor indicates the effectiveness of the Modified FDs in reducing the contribution of higher mode responses to the total dynamic response of the building model.

Summary

This study (1) explored the design space and determined one set of the design parameters of the modified friction-based force-limiting connection (Modified FD); and (2) assessed the seismic response of a 3D 18-story core wall building model with the Modified FDs. The one set of the design parameters of the Modified FD that resulted in an improved seismic response of a building model was determined using Pareto front analysis. The Pareto front analysis utilized results from systematic parametric numerical earthquake simulations of 2D building models and results from a practical force-based design method for force-limiting connections. A 3D model of an 18-story reinforced concrete core wall building was developed with experimentally calibrated wall piers and the Modified FDs

Downloaded from ascelibrary.org by University of California, San Diego on 12/17/24. Copyright ASCE. For personal use only; all rights reserved.

considering the determined set of design parameters. Numerical earthquake simulations of the 3D 18-story reinforced concrete core wall building were performed considering 13 design-level far-field bidirectional ground motions. The seismic response of the building model with the Modified FDs was compared with the seismic response of the building model with conventional monolithic connections (RE connections), the seismic response of the building model with force-limiting connections developed for buildings with planar SFRS (FD+RBs), and the seismic response of the building model with force-limiting connections with only friction devices and no rubber bearings (FDs). The comparative analysis was performed focusing on the floor total acceleration, SFRS story shear, SFRS story torsional moment, story drift ratio, story torsional drift ratio, residual drift ratio responses, and the maximum and minimum strain responses at the wall base. A detailed assessment of the higher-mode effects in the total dynamic response of the building was performed.

Conclusions

Based on the study results, the following conclusions were made:

- The Pareto front analysis can be used to determine a set of design parameters of the Modified FDs that result in an improved seismic response of a building model. The determined values of the parameters R_{DC}, D_1, D_2, F_2, and F_3 are 2.00, 12.7 mm, 25.4 mm, $0.375F_{Lx}$, and $0.5F_{Lx}$, respectively. The use of the force-based design method leads to a reasonable estimate for F_{Lx}.
- The use of the Modified FDs in the 18-story core wall building model reduced the magnitude in the peak values of the floor total acceleration, SFRS base shear, and SFRS base torsional moment by 40%, 33%, and 46%, respectively, compared to those from the building model with conventional monolithic connections.
- The use of the Modified FDs in the 18-story core wall building model reduced the variability in the peak values of the floor total acceleration, SFRS base shear, and SFRS base torsional moment by 77%, 68%, and 76%, respectively, compared to those from the building model with conventional monolithic connections.
- The use of the Modified FDs in the 18-story core wall building model resulted in the peak values of the SFRS story drift ratio, GLRS story drift ratio, and GLRS story torsional drift ratio responses similar to those from the building model with conventional monolithic connections.
- The use of the Modified FDs in the 18-story core wall building model resulted in reduced mean SFRS residual drift ratio compared to those from the building model with conventional monolithic connections. The use of the Modified FDs in the 18-story core wall building model resulted in reduced mean GLRS residual drift ratio near the roof, increased mean GLRS residual drift ratio near the base, and a similar maximum mean GLRS residual drift ratio, compared to those from the building model with conventional monolithic connections.
- The use of the Modified FDs in the 18-story core wall building model reduced the magnitude in the absolute values of the maximum and minimum strain responses at the wall base by 41% and 35%, respectively, compared to those from the building model with conventional monolithic connections. In addition, the use of the Modified FDs in the 18-story core wall building model reduced the variability in the absolute values of the maximum and minimum strain responses at the wall base by 55% and 63%, respectively, compared to those from the building model with conventional monolithic connections.
- The use of the Modified FDs in the 18-story core wall building model resulted in peak values of the connection deformation response similar to those from the building model with the FD+RBs, which were smaller than those from the building model with the FDs. Therefore, the predetermined discrete variable limiting force of the Modified FD prevents excessive connection deformation demands without the need for low-damping rubber bearings used in the force-limiting connection for buildings with planar SFRS.
- The controlled inelastic force-displacement response of the Modified FDs modifies the instantaneous state of stiffness and the instantaneous dynamic properties of the structural system. As a result, the use of the Modified FDs limits the magnitude and variability in the shear-dominant higher-mode-induced acceleration and force responses.

Data Availability Statement

Some or all data, models, or code that support the findings of this study are available from the corresponding author upon reasonable request.

Acknowledgments

The authors are grateful for the financial support provided by the University of California San Diego. Any opinions, findings, and conclusions expressed in this paper are those of the authors and do not necessarily reflect the views of others acknowledged here.

Author contributions: Kyoungyeon Lee conducted literature reviews, performed the Pareto front analysis using data derived from parametric numerical earthquake simulations, performed numerical earthquake simulations of the 3D 18-story core wall building model, interpreted the numerical results, created figures, and wrote the manuscript. Georgios Tsampras conceived the research project, provided major guidance throughout the research process, interpreted the numerical results, and co-wrote and revised the manuscript. C. Franco Mayorga performed the parametric numerical earthquake simulations of the simplified 2D 18-story planar wall building model, and revised the manuscript.

References

ACI (American Concrete Institute). 2014. *Building code requirements for structural concrete and commentary.* ACI 318-14. Farmington Hills, MI: ACI.

ACI (American Concrete Institute). 2019. *Building code requirements for structural concrete and commentary.* ACI 318-19. Farmington Hills, MI: ACI.

Ali, M. M., and K. S. Moon. 2007. "Structural developments in tall buildings: Current trends and future prospects." *Archit. Sci. Rev.* 50 (3): 205–223. https://doi.org/10.3763/asre.2007.5027.

Arora, J. S. 2017. *Introduction to optimum design*. 4th ed. Boston: Academic Press.

ASCE. 2016. *Minimum design loads and associated criteria for buildings and other structures*. ASCE 7-16. Reston, VA: ASCE.

ASCE. 2022. *Minimum design loads and associated criteria for buildings and other structures*. ASCE 7-22. Reston, VA: ASCE.

Baker, J. W. 2011. "Conditional mean spectrum: Tool for ground-motion selection." *J. Struct. Eng.* 137 (3): 322–331. https://doi.org/10.1061/(ASCE)ST.1943-541X.0000215.

Beyer, K., A. Dazio, and M. J. N. Priestley. 2008. "Quasi-static cyclic tests of two U-shaped reinforced concrete walls." *J. Earthquake Eng.* 12 (7): 1023–1053. https://doi.org/10.1080/13632460802003272.

Downloaded from ascelibrary.org by University of California, San Diego on 12/17/24. Copyright ASCE. For personal use only; all rights reserved.

Birrell, M., R. Astroza, R. Carreño, J. I. Restrepo, and G. Araya-Letelier. 2021. "Bayesian parameter and joint probability distribution estimation for a hysteretic constitutive model of reinforcing steel." *Struct. Saf.* 90 (May): 102062. https://doi.org/10.1016/j.strusafe.2020.102062.

Boore, D. M. 2010. "Orientation-independent, nongeometric-mean measures of seismic intensity from two horizontal components of motion." *Bull. Seismol. Soc. Am.* 100 (4): 1830–1835. https://doi.org/10.1785/0120090400.

Calugaru, V. 2013. "Earthquake resilient tall reinforced concrete buildings at near-fault sites using base isolation and rocking core walls." Ph.D. thesis, Dept. of Civil and Environmental Engineering, Univ. of California, Berkeley.

Calugaru, V., and M. Panagiotou. 2012. "Response of tall cantilever wall buildings to strong pulse type seismic excitation." *Earthquake Eng. Struct. Dyn.* 41 (9): 1301–1318. https://doi.org/10.1002/eqe.1185.

Calugaru, V., and M. Panagiotou. 2014. "Seismic response of 20-story base-isolated and fixed-base reinforced concrete structural wall buildings at a near-fault site." *Earthquake Eng. Struct. Dyn.* 43 (6): 927–948. https://doi.org/10.1002/eqe.2381.

Chen, K., G. Tsampras, and K. Lee. 2023. "Structural connection with predetermined discrete variable friction forces." *Resilient Cities Struct.* 2 (1): 1–17. https://doi.org/10.1016/j.rcns.2023.02.006.

Chen, K., G. Tsampras, K. Lee, and C. F. Mayorga. 2022. "Reusable force-limiting connection with variable friction force for high-performance buildings." In *Proc., 8th Asia Conf. on Earthquake Engineering (8ACEE)*. Taipei, Taiwan: National Science and Technology Council.

Christopoulos, C., and M. Montgomery. 2013. "Viscoelastic coupling dampers (VCDs) for enhanced wind and seismic performance of high-rise buildings." *Earthquake Eng. Struct. Dyn.* 42 (15): 2217–2233. https://doi.org/10.1002/eqe.2321.

Christopoulos, C., and C. Zhong. 2022. "Towards understanding, estimating and mitigating higher-mode effects for more resilient tall buildings." *Resilient Cities Struct.* 1 (1): 53–64. https://doi.org/10.1016/j.rcns.2022.03.005.

Chung, H.-S., B.-W. Moon, S.-K. Lee, J.-H. Park, and K.-W. Min. 2009. "Seismic performance of friction dampers using flexure of RC shear wall system." *Struct. Des. Tall Special Build.* 18 (7): 807–822. https://doi.org/10.1002/tal.524.

Coleman, J., and E. Spacone. 2001. "Localization issues in force-based frame elements." *J. Struct. Eng.* 127 (11): 1257–1265. https://doi.org/10.1061/(ASCE)0733-9445(2001)127:11(1257).

Crane, S. T. 2004. "Influence of energy dissipation connections between floors and the lateral force resisting system." M.S. thesis, Dept. of Structural Engineering, Univ. of California, San Diego.

Cui, Y., Q. Tang, T. Wu, T. Okazaki, and T. Wang. 2022a. "Mechanism and experimental validation of frictional steel truss coupling beams." *J. Struct. Eng.* 148 (9): 04022129. https://doi.org/10.1061/(ASCE)ST.1943-541X.0003420.

Cui, Y., Q. Tang, T. Wu, and T. Wang. 2022b. "Seismic performance of bending-type frictional steel truss coupling beams." *Earthquake Eng. Struct. Dyn.* 51 (3): 673–687. https://doi.org/10.1002/eqe.3585.

Deierlein, G., A. Reinhorn, and M. Willford. 2010. *NEHRP seismic design technical brief No. 4—Nonlinear structural analysis for seismic design: A guide for practicing engineers*. Grant/Contract Reports (NISTGCR). Gaithersburg, MD: NIST.

Fatemi, H., P. Paultre, and C.-P. Lamarche. 2020. "Experimental evaluation of inelastic higher-mode effects on the seismic behavior of RC structural walls." *J. Struct. Eng.* 146 (4): 04020016. https://doi.org/10.1061/(ASCE)ST.1943-541X.0002509.

FEMA. 2009. *Quantification of building seismic performance factors*. FEMA P695. Washington, DC: FEMA.

Filippou, F. C., E. P. Popov, and V. V. Bertero. 1983. *Effects of bond deterioration on hysteretic behavior of reinforced concrete joints*. Richmond, CA: Earthquake Engineering Research Center.

Fleischman, R., J. Restrepo, A. Nema, D. Zhang, U. Shakya, Z. Zhang, R. Sause, G. Tsampras, and G. Monti. 2015. "Inertial force-limiting anchorage system for seismic resistant building structures." In *Proc., Structures Congress 2015*. Reston, VA: ASCE.

Fleischman, R. B., J. I. Restrepo, R. Sause, D. Zhang, G. Tsampras, Z. Zhang, A. Nema, and U. Shakya. 2014. *Half scale shake table test of a 4 story reinforced concrete building with eccentric shear walls*. Alexandria, VA: National Science Foundation.

Johnston, H., C. Watson, S. Pampanin, and A. Palermo. 2014. "Shake table testing of an integrated low damage building system." In *Proc., 2nd European Conf. on Earthquake Engineering and Seismology*. Istanbul, Turkey: European Association for Earthquake Engineering.

Kent, D. C., and R. Park. 1971. "Flexural members with confined concrete." *J. Struct. Div.* 97 (7): 1969–1990. https://doi.org/10.1061/JSDEAG.0002957.

Kent, J., C. Zhong, and C. Christopoulos. 2023. "Steel flexure and shear yielding base-mechanism for enhanced seismic resilience of RC core wall high-rise structures." *Earthquake Spectra* 39 (1): 148–170. https://doi.org/10.1177/87552930221132862.

Key, D. E. 1984. "The seismic performance of energy absorbing dampers in building structures." *Bull. N. Z. Soc. Earthquake Eng.* 17 (1): 38–46. https://doi.org/10.5459/bnzsee.17.1.38-46.

Komuro, T., Y. Nishikawa, Y. Kimura, and Y. Isshiki. 2005. "Development and realization of base isolation system for high-rise buildings." *J. Adv. Concr. Technol.* 3 (2): 233–239. https://doi.org/10.3151/jact.3.233.

LATBSDC (Los Angeles Tall Buildings Structural Design). 2020. *An alternative procedure for seismic analysis and design of tall buildings located in the Los Angeles region*. Los Angeles: LATBSDC.

Lee, K., K. Chen, and G. Tsampras. 2022. "Seismic response of core wall building with friction-based force-limiting connections." In *Proc., 3rd European Conf. on Earthquake Engineering & Seismology (3ECEES)*. Bucharest, Romania: Editura Conspress.

Li, S., H. Jiang, and L. He. 2019. "Study of a new type of replaceable coupling beam in reinforced concrete shear wall structures." *Struct. Des. Tall Special Build.* 28 (10): e1620. https://doi.org/10.1002/tal.1620.

Luco, J. E., and F. C. P. De Barros. 1998. "Control of the seismic response of a composite tall building modelled by two interconnected shear beams." *Earthquake Eng. Struct. Dyn.* 27 (3): 205–223. https://doi.org/10.1002/(SICI)1096-9845(199803)27:3<205::AID-EQE712>3.0.CO;2-X.

Mander, J. B., M. J. N. Priestley, and R. Park. 1988. "Theoretical stress-strain model for confined concrete." *J. Struct. Eng.* 114 (8): 1804–1826. https://doi.org/10.1061/(ASCE)0733-9445(1988)114:8(1804).

Mar, D., and S. Tipping. 2000. *Smart frame story isolation system: A new high-performance seismic technology*. Berkeley, CA: Tipping Mar and Associates.

Mayorga, C. F., K. Lee, and G. Tsampras. 2022. "Effect of the structural wall modeling in the seismic response of buildings with force-limiting connections between diaphragm-to-wall joints." In *Proc., Engineering Mechanics Institute (EMI) Conf.* Reston, VA: ASCE.

Mayorga, C. F., and G. Tsampras. 2024. "Reinforced concrete wall buildings with force-limiting connections: Modeling effects and uncertainty propagation." *Earthquake Eng. Struct. Dyn.* 53 (4): 1465–1491. https://doi.org/10.1002/eqe.4073.

McKenna, F., M. H. Scott, and G. L. Fenves. 2010. "Nonlinear finite-element analysis software architecture using object composition." *J. Comput. Civ. Eng.* 24 (1): 95–107. https://doi.org/10.1061/(ASCE)CP.1943-5487.0000002.

Menegotto, M., and P. E. Pinto. 1973. "Method of analysis for cyclically loaded R.C. plane frames including changes in geometry and non-elastic behaviour of elements under combined normal force and bending." In *Proc., IABSE Symp. on Resistance and Ultimate Deformability of Structures Acted on by Well Defined Repeated Loads*. Zurich, Switzerland: IABSE.

Moehle, J. P. 2006. "Seismic analysis, design, and review for tall buildings." *Struct. Design Tall Special Build.* 15 (5): 495–513. https://doi.org/10.1002/tal.378.

Moehle, J. P. 2014. *Seismic design of reinforced concrete buildings*. New York: McGraw-Hill Professional.

Moehle, J. P., T. Ghodsi, J. D. Hooper, D. C. Fields, and R. Gedhada. 2011. *NEHRP seismic design technical brief no. 6—Seismic design of cast-in-place concrete special structural walls and coupling beams: A guide for practicing engineers*. Gaithersburg, MD: NIST.

Mohd Yassin, M. H. 1994. "Nonlinear analysis of prestressed concrete structures under monotonic and cyclic loads." Ph.D. thesis, Dept. of Civil Engineering, Univ. of California, Berkeley.

Downloaded from ascelibrary.org by University of California, San Diego on 12/17/24. Copyright ASCE. For personal use only; all rights reserved.

Panagiotou, M., and J. I. Restrepo. 2009. "Dual-plastic hinge design concept for reducing higher-mode effects on high-rise cantilever wall buildings." *Earthquake Eng. Struct. Dyn.* 38 (12): 1359–1380. https://doi.org/10.1002/eqe.905.

Panneton, M., P. Léger, and R. Tremblay. 2006. "Inelastic analysis of a reinforced concrete shear wall building according to the National Building Code of Canada 2005." *Can. J. Civ. Eng.* 33 (7): 854–871. https://doi.org/10.1139/l06-026.

Paulay, T., and M. J. N. Priestley. 1992. *Seismic design of reinforced concrete and masonry buildings*. New York: Wiley.

Pennucci, D., T. J. Sullivan, and G. M. Calvi. 2015. "Inelastic higher-mode response in reinforced concrete wall structures." *Earthquake Spectra* 31 (3): 1493–1514. https://doi.org/10.1193/051213EQS123M.

Priestley, M. J. N., G. M. Calvi, and M. J. Kowalsky. 2007. *Displacement based seismic design of structures*. Pavia, Italy: IUSS Press.

Qu, Z., X. Ji, X. Shi, Y. Wang, and H. Liu. 2020. "Cyclic loading test of steel coupling beams with mid-span friction dampers and RC slabs." *Eng. Struct.* 203 (Jan): 109876. https://doi.org/10.1016/j.engstruct.2019.109876.

Skinner, R. I., J. M. Kelly, and A. J. Heine. 1974. "Hysteretic dampers for earthquake-resistant structures." *Earthquake Eng. Struct. Dyn.* 3 (3): 287–296. https://doi.org/10.1002/eqe.4290030307.

Tauberg, N. A., K. Kolozvari, and J. W. Wallace. 2019. *Ductile reinforced concrete coupled walls: FEMA P695 study.* Los Angeles: UCLA Structural/Earthquake Engineering Research Laboratory.

Tong, F., and C. Christopoulos. 2020. "Uncoupled rocking and shear base-mechanisms for resilient reinforced concrete high-rise buildings." *Earthquake Eng. Struct. Dyn.* 49 (10): 981–1006. https://doi.org/10.1002/eqe.3273.

Tong, F., and C. Christopoulos. 2021. "Insights on higher-mode effects in high-rise buildings with flexible base rotational and translational restraints: A theoretical study using a continuum beam analogy." *J. Earthquake Eng.* 27 (2): 314–339. https://doi.org/10.1080/13632469.2021.2001394.

Tsampras, G., and R. Sause. 2014a. *Full-scale, components test of inertial force-limiting floor anchorage systems for seismic resistant building structures using a buckling restrained brace and steel reinforced low damping rubber bearings*. Alexandria, VA: National Science Foundation.

Tsampras, G., and R. Sause. 2014b. *Full-scale, components test of inertial force-limiting floor anchorage systems for seismic resistant building structures using a friction device and carbon fiber reinforced low damping rubber bearings*. Alexandria, VA: National Science Foundation.

Tsampras, G., and R. Sause. 2022. "Force-based design method for force-limiting deformable connections in earthquake-resistant buildings." *J. Struct. Eng.* 148 (10): 04022150. https://doi.org/10.1061/(ASCE)ST.1943-541X.0003456.

Tsampras, G., R. Sause, R. B. Fleischman, and J. I. Restrepo. 2016a. "Experimental study of deformable connection consisting of buckling-restrained brace and rubber bearings to connect floor system to lateral force resisting system." *Earthquake Eng. Struct. Dyn.* 46 (8): 1287–1305. https://doi.org/10.1002/eqe.2856.

Tsampras, G., R. Sause, R. B. Fleischman, and J. I. Restrepo. 2017. "Experimental study of deformable connection consisting of friction device and rubber bearings to connect floor system to lateral force resisting system." *Earthquake Eng. Struct. Dyn.* 47 (4): 1032–1053. https://doi.org/10.1002/eqe.3004.

Tsampras, G., R. Sause, D. Zhang, R. B. Fleischman, J. I. Restrepo, D. Mar, and J. Maffei. 2016b. "Development of deformable connection for earthquake-resistant buildings to reduce floor accelerations and force responses." *Earthquake Eng. Struct. Dyn.* 45 (9): 1473–1494. https://doi.org/10.1002/eqe.2718.

Wiebe, L., and C. Christopoulos. 2009. "Mitigation of higher mode effects in base-rocking systems by using multiple rocking sections." *J. Earthquake Eng.* 13 (1): 83–108. https://doi.org/10.1080/13632460902813315.

Wiebe, L., C. Christopoulos, R. Tremblay, and M. Leclerc. 2013a. "Mechanisms to limit higher mode effects in a controlled rocking steel frame. 1: Concept, modelling, and low-amplitude shake table testing." *Earthquake Eng. Struct. Dyn.* 42 (7): 1053–1068. https://doi.org/10.1002/eqe.2259.

Wiebe, L., C. Christopoulos, R. Tremblay, and M. Leclerc. 2013b. "Mechanisms to limit higher mode effects in a controlled rocking steel frame. 2: Large-amplitude shake table testing." *Earthquake Eng. Struct. Dyn.* 42 (7): 1069–1086. https://doi.org/10.1002/eqe.2258.

Zhang, Z., R. B. Fleischman, J. I. Restrepo, G. Guerrini, A. Nema, D. Zhang, U. Shakya, G. Tsampras, and R. Sause. 2018. "Shake-table test performance of an inertial force-limiting floor anchorage system." *Earthquake Eng. Struct. Dyn.* 47 (10): 1987–2011. https://doi.org/10.1002/eqe.3047.

Zhong, C., and C. Christopoulos. 2022a. "Self-centering seismic-resistant structures: Historical overview and state-of-the-art." *Earthquake Spectra* 38 (2): 1321–1356. https://doi.org/10.1177/87552930211057581.

Zhong, C., and C. Christopoulos. 2022b. "Shear-controlling rocking-isolation podium system for enhanced resilience of high-rise buildings." *Earthquake Eng. Struct. Dyn.* 51 (6): 1363–1382. https://doi.org/10.1002/eqe.3619.

Zhong, C., and C. Christopoulos. 2023a. "Seismic response of slender MDOF structures with self-centering base shear and moment mechanisms." *Earthquake Eng. Struct. Dyn.* 52 (6): 1658–1677. https://doi.org/10.1002/eqe.3834.

Zhong, C., and C. Christopoulos. 2023b. "Shake table testing of shear-controlling rocking isolation podium system for mitigating higher-mode effects in tall buildings." *J. Struct. Eng.* 149 (5): 04023026. https://doi.org/10.1061/JSENDH.STENG-12000.

Downloaded from ascelibrary.org by University of California, San Diego on 12/17/24. Copyright ASCE. For personal use only; all rights reserved.